

Graph-enhanced Optimizers for Structure-aware Recommendation Embedding Evolution

Cong Xu

East China Normal University
Shanghai, China
cong Xu@icloud.com

Jianyong Wang

Tsinghua University
Beijing, China
jianyong@tsinghua.edu.cn

Jun Wang

East China Normal University
Shanghai, China
wongjun@gmail.com

Wei Zhang

East China Normal University
Shanghai, China
zhangwei.thu2011@gmail.com

ABSTRACT

Embedding plays a critical role in modern recommender systems because they are virtual representations of real-world entities and the foundation for subsequent decision models. In this paper, we propose a novel embedding update mechanism, Structure-aware Embedding Evolution (SEvo for short), to encourage related nodes to evolve similarly at each step. Unlike GNN (Graph Neural Network) that typically serves as an intermediate part, SEvo is able to directly inject the graph structure information into embedding with negligible computational overhead in training. The convergence properties of SEvo as well as its possible variants are theoretically analyzed to justify the validity of the designs. Moreover, SEvo can be seamlessly integrated into existing optimizers for state-of-the-art performance. In particular, SEvo-enhanced AdamW with moment estimate correction demonstrates consistent improvements across a spectrum of models and datasets, suggesting a novel technical route to effectively utilize graph structure information beyond explicit GNN modules. Our code is available at <https://github.com/MTandHJ/SEvo>.

CCS CONCEPTS

• **Information systems** → **Recommender systems**; • **Computer systems organization** → **Neural networks**.

KEYWORDS

recommendation, optimization, graph neural networks, embedding

ACM Reference Format:

Cong Xu, Jun Wang, Jianyong Wang, and Wei Zhang. 2024. Graph-enhanced Optimizers for Structure-aware Recommendation Embedding Evolution. In *Proceedings of ACM Conference (Conference'17)*. ACM, New York, NY, USA, 19 pages. <https://doi.org/XXXXXXX.XXXXXXX>

Permission to make digital or hard copies of all or part of this work for personal or classroom use is granted without fee provided that copies are not made or distributed for profit or commercial advantage and that copies bear this notice and the full citation on the first page. Copyrights for components of this work owned by others than ACM must be honored. Abstracting with credit is permitted. To copy otherwise, or republish, to post on servers or to redistribute to lists, requires prior specific permission and/or a fee. Request permissions from permissions@acm.org.
Conference'17, July 2017, Washington, DC, USA

© 2024 Association for Computing Machinery.
ACM ISBN 978-1-4503-XXXX-X/18/06...\$15.00
<https://doi.org/XXXXXXX.XXXXXXX>

1 INTRODUCTION

Surfing Internet leaves footprints such as clicks [14], browsing [4], and shopping histories [53]. For a modern recommender system [5, 11], the entities involved (*e.g.*, goods, movies) are typically embedded into a latent space based on these interaction data. As the embedding takes the most to construct and is the foundation to subsequent decision models, its modeling quality directly determines the final performance of the entire system. According to the homophily assumption [30, 54], it is natural to expect that related entities have closer representations in the latent space. Note that the similarity between two entities refers specifically to those extracted from interaction data [44] or prior knowledge [35]. For example, goods selected consecutively by the same user, or movies of the same genre, often tend to be perceived as more relevant. Graph neural networks (GNNs) [2, 9, 13] are a popular technique to exploit such structure information, in concert with a weighted adjacency matrix wherein each entry characterizes how closely two nodes are related. Rather than directly injecting structure information into embedding, GNN typically serves as an intermediate part in the recommender. However, designing a versatile GNN module suitable for various recommendation scenarios is challenging. This is especially true for sequential recommendation [7, 48], which needs to take into account both structure and sequence information. Moreover, the post-processing fashion inevitably increases the overhead of training and inference, limiting the scalability for real-time recommendation.

In this work, we aim to directly inject graph structure information into embedding through a novel embedding update mechanism. Figure 1a illustrates a normal embedding evolution process, in which the embedding \mathbf{E} is updated at step t by

$$\mathbf{E}_t \leftarrow \mathbf{E}_{t-1} + \Delta \mathbf{E}_{t-1}.$$

Note that the variation $\Delta \mathbf{E}$ is mainly determined by the (anti-)gradient. It points to a region able to decrease a loss function concerning recommendation performance [33], but lacks an explicit guarantee that the variations between related nodes are similar. The embeddings thus cannot be expected to satisfactorily model pairwise relations while minimizing the recommendation loss.

Conversely, structure information can be learned if related nodes evolve similarly at each update. The structure-aware embedding evolution (SEvo for short), shown in Figure 1b, is developed for this

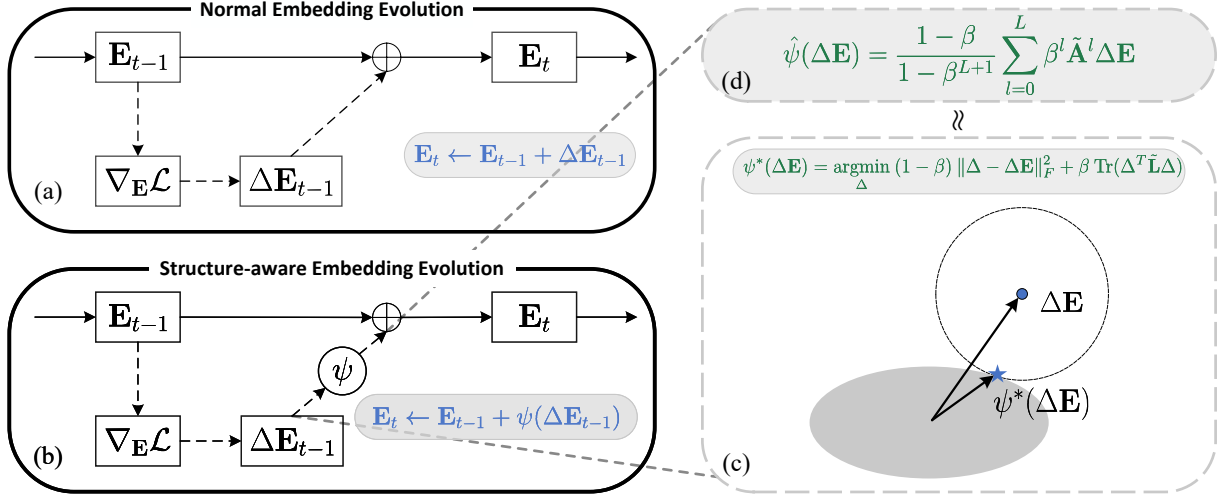


Figure 1: Overview of SEvo. (a) Normal embedding evolution. (b) (Section 2) Structure-aware embedding evolution. (c) (Section 2.2) Geometric visualization of the variation from $\Delta \mathbf{E}$ to $\psi^*(\Delta \mathbf{E})$. The gray ellipse represents the region with proper smoothness. (d) (Section 2.3) The L -layer approximation with a faster convergence guarantee.

goal. A special transformation is applied so as to meet both smoothness and convergence [52]. Because these two criteria inherently conflict to some extent, we resort to a graph regularization framework [6, 52] to balance them. While analogous frameworks have been used to understand feature smoothing and modify message passing mechanisms for GNNs [27, 55], applying this to variations is not as straightforward as to features [23] or labels [18]. Previous efforts are capable of smoothing, but cannot account for strict convergence. The specific transformation form must be chosen carefully; subtle differences may slow down or even kill training. Through an exhaustive theoretical analysis, we develop an applicable solution with a provable convergence guarantee.

Apart from the anti-gradient, the variation $\Delta \mathbf{E}$ can also be derived from the moment estimates. Therefore, existing optimizers, such as SGD [39] and Adam [22], can benefit from SEvo readily. In contrast to Adam, AdamW [26] decouples the weight decay from the optimization step, thereby more suitable here since it makes no sense to require the weight decay to be smooth as well. Furthermore, we recorrect the moment estimates of SEvo-enhanced AdamW when encountering sparse gradients. This modification allows it to be more robust to a variety of recommendation models and scenarios. Numerous experiments over four public datasets have demonstrated that it can effectively inject structure information to boost recommendation performance. Since SEvo does not change the inference logic of the model, the inference time is exactly the same, and only negligible computational overhead is required during training.

The main contributions of this paper are summarized below.

- The graph regularization framework [6, 52] has been widely used for feature/label smoothing. To best of our knowledge, we are the first to apply it to variations as an alternative to explicit GNN

modules for recommendation. The final transformation is not trivial and comes from exhaustive theoretical analyses.

- We present SEvo-enhanced AdamW by incorporating SEvo and recorrecting the original moment estimates. These modifications demonstrate consistent performance, with 9%~23% average improvements across a spectrum of models. Other optimizers such as SGD and Adam can be performed in a similar way with SEvo.
- In addition to interaction data, we preliminarily explore the pairwise similarity estimation based on other prior knowledge: node categories to promote intra-class representation proximity, and knowledge distillation [17] to encourage a light-weight student to mimic the embedding behaviors of a teacher model. It showcases SEvo’s versatility.

The remainder of this paper is organized as follows. Structure-aware embedding evolution and its convergence analysis are detailed in Section 2. We then introduce in Section 3 how to integrate SEvo into existing optimizers. Section 4 complements the experimental results based on interaction data, while the application of SEvo to other prior knowledge are explored in Appendix D.

2 STRUCTURE-AWARE EMBEDDING EVOLUTION

In this section, we first introduce some necessary terminology and concepts, in particular smoothness. SEvo and its theoretical analyses will be detailed in Section 2.2 and 2.3. The proofs hereafter are deferred to Appendix A.

2.1 Preliminaries

Notations and terminology. Let $\mathcal{V} = \{v_1, \dots, v_n\}$ denote a set of nodes and $\mathbf{A} = [w_{ij}] \in \mathbb{R}^{n \times n}$ a symmetric adjacency matrix, where each entry $w_{ij} = w_{ji}$ characterizes how closely v_i and v_j are related.

They jointly constitute the graph $\mathcal{G} = (\mathcal{V}, \mathbf{A})$. For example, \mathcal{V} could be a set of movies, and w_{ij} is the frequency of v_i and v_j being liked by the same user. Denoted by $\mathbf{D} \in \mathbb{R}^{n \times n}$ the diagonal degree matrix of \mathbf{A} , the normalized adjacency matrix and the corresponding Laplacian matrix are defined as $\tilde{\mathbf{A}} = \mathbf{D}^{-1/2} \mathbf{A} \mathbf{D}^{-1/2}$ and $\tilde{\mathbf{L}} = \mathbf{I} - \tilde{\mathbf{A}}$, respectively. For ease of notation, we use $\langle \cdot, \cdot \rangle$ to denote the inner product, $\langle \mathbf{x}, \mathbf{y} \rangle = \mathbf{x}^T \mathbf{y}$ for vectors and $\langle \mathbf{X}, \mathbf{Y} \rangle = \text{Tr}(\mathbf{X}^T \mathbf{Y})$ for matrices. Here, $\text{Tr}(\cdot)$ denotes the trace of a given matrix.

Smoothness. Before delving into the details of SEvo, it is necessary to present a metric to measure the smoothness [6, 52] of node features \mathbf{X} as a whole. Denoted by $\mathbf{x}_i, \mathbf{x}_j$ the row vectors of \mathbf{X} and $d_i = \sum_j w_{ij}$, we have

$$\begin{aligned} \mathcal{J}_{\text{smoothness}}(\mathbf{X}; \mathcal{G}) &:= \text{Tr}(\mathbf{X}^T \tilde{\mathbf{L}} \mathbf{X}) \\ &= \sum_{i,j \in \mathcal{V}} w_{ij} \left\| \frac{\mathbf{x}_i}{\sqrt{d_i}} - \frac{\mathbf{x}_j}{\sqrt{d_j}} \right\|_2^2. \end{aligned} \quad (1)$$

This term is often used as graph regularization for feature/label smoothing [18, 23]. Intuitively, a lower $\mathcal{J}_{\text{smoothness}}$ indicates smaller difference between closely related pairs of nodes, and in this case \mathbf{X} is considered smoother. However, smoothness alone is not sufficient from a performance perspective. Over-emphasizing this indicator instead leads to the well-known over-smoothing issue [25]. How to balance variation smoothness and convergence is the main challenge to be addressed below.

2.2 Methodology

The entities involved in a recommender system are typically embedded into a latent space [5, 11], and the embeddings in $\mathbf{E} \in \mathbb{R}^{n \times d}$ are expected to be smooth so that related nodes are close to each other. In general, \mathbf{E} is learnable and updated at step t by

$$\mathbf{E}_t \leftarrow \mathbf{E}_{t-1} + \Delta \mathbf{E}_{t-1},$$

where the variation $\Delta \mathbf{E}$ is mainly determined by the (anti-)gradient. For example, $\Delta \mathbf{E} = -\eta \nabla_{\mathbf{E}} \mathcal{L}$ when gradient descent with a learning rate of η is used to minimize a loss function \mathcal{L} . However, the final embeddings based on this evolution process may be far from sufficient smoothness because: 1) The variation $\Delta \mathbf{E}$ points to the region able to decrease the loss function concerning recommendation performance, but lacks an explicit smoothness guarantee. 2) The variations of two related nodes may be quite different due to the randomness from initialization and mini-batch sampling.

We are to design a special transformation $\psi(\cdot)$ to smooth the variation so that the evolution deduced from the following update formula is structure-aware,

$$\mathbf{E}_t \leftarrow \mathbf{E}_{t-1} + \psi(\Delta \mathbf{E}_{t-1}). \quad (2)$$

Recall that, in this paper, the similarity is confined to quantifiable values in the adjacency matrix \mathbf{A} , in which more related pairs are weighted higher. Therefore, this transformation should encourage pairs of nodes connected with higher weights to evolve more similarly than those connected with lower weights. This can be boiled down to structure-aware transformation as defined below.

DEFINITION 1 (STRUCTURE-AWARE TRANSFORMATION). *The transformation $\psi(\cdot)$ is structure-aware if*

$$\mathcal{J}_{\text{smoothness}}(\psi(\Delta \mathbf{E})) \leq \mathcal{J}_{\text{smoothness}}(\Delta \mathbf{E}). \quad (3)$$

On the other hand, this transformation must ensure convergence throughout the evolution process, which means that the transformed variation should not differ too much from the original. For the sake of theoretical analysis, the ability to maintain the update direction will be used to qualitatively depict this desirable property below, though a quantitative squared error will be employed later.

DEFINITION 2 (DIRECTION-AWARE TRANSFORMATION). *The transformation $\psi(\cdot)$ is direction-aware if*

$$\langle \psi(\Delta \mathbf{E}), \Delta \mathbf{E} \rangle > 0, \quad \forall \Delta \mathbf{E} \neq \mathbf{0}. \quad (4)$$

These two criteria inherently conflict to some extent. We resort to a hyperparameter $\beta \in [0, 1)$ to make a trade-off and the desired transformation is the corresponding minimum; that is ($\|\cdot\|_F$ denotes the the Frobenius norm),

$$\psi^*(\Delta \mathbf{E}; \beta) = \underset{\Delta}{\text{argmin}} (1 - \beta) \|\Delta - \Delta \mathbf{E}\|_F^2 + \beta \underbrace{\text{Tr}(\Delta^T \tilde{\mathbf{L}} \Delta)}_{\mathcal{J}_{\text{smoothness}}}. \quad (5)$$

A larger β indicates a stronger smoothness constraint and $\psi^*(\Delta \mathbf{E})$ reduces to $\Delta \mathbf{E}$ when $\beta \rightarrow 0$. Geometrically, as shown in Figure 1c, $\psi^*(\Delta \mathbf{E})$ can be understood as a projection of $\Delta \mathbf{E}$ onto the region with proper smoothness. Taking the gradient to zero gives a closed-form solution:

$$\psi^*(\Delta \mathbf{E}) = (1 - \beta)(\mathbf{I} - \beta \tilde{\mathbf{A}})^{-1} \Delta \mathbf{E}.$$

However, exact matrix inversion requires $\mathcal{O}(|\mathcal{V}|^3)$ arithmetic operations and $\mathcal{O}(|\mathcal{V}|^3)$ memory overhead, which is prohibitively expensive in recommendation due to the large number of entities. Zhou et al. [52] suggested a L -layer iterative approximation to circumvent this problem:

$$\begin{aligned} \hat{\psi}_{\text{iter}}(\Delta \mathbf{E}) &:= \hat{\psi}_L(\Delta \mathbf{E}), \\ \hat{\psi}_l(\Delta \mathbf{E}) &= \beta \tilde{\mathbf{A}} \hat{\psi}_{l-1}(\Delta \mathbf{E}) + (1 - \beta) \Delta \mathbf{E}, \\ \hat{\psi}_0(\Delta \mathbf{E}) &= \Delta \mathbf{E}. \end{aligned}$$

The resulting transformation is actually a momentum update that aggregates higher-order information layer by layer. Analogous message-passing mechanisms have been used in previous GNNs such as APPNP [23] and C&S [18]. However, this commonly used approximate solution is not compatible with SEvo; sometimes, variations after the transformation may be opposite to the original direction, leading to a failure of convergence.

THEOREM 2.1. *The iterative approximation is direction-aware for all possible normalized adjacency matrices and $L \geq 0$, if and only if $\beta < 1/2$. In contrast, the Neumann series approximation*

$$\hat{\psi}_{\text{nsa}}(\Delta \mathbf{E}) = (1 - \beta) \sum_{l=0}^L \beta^l \tilde{\mathbf{A}}^l \Delta \mathbf{E}, \quad (6)$$

is structure-aware and direction-aware for any $\beta \in [0, 1)$.

As suggested in Theorem 2.1, a compromise is to restrict β to $[0, 1/2)$ for $\hat{\psi}_{\text{iter}}$, but this may lead to a lack of smoothness. The Neumann series approximation [37] of Eq. (6) seems to be a viable alternative; qualitatively, it satisfies both desirable properties. Nevertheless, this transformation can be further modified for a faster convergence rate based on the analysis presented next.

Table 1: Summary of different forms of transformations.

Transformation	Structure-aware	Direction-aware	Convergence rate
$\hat{\psi}_{iter}$	✓		
$\hat{\psi}_{nsa}$	✓	✓	$O(C/((1-\beta)^2T))$
$\hat{\psi}$	✓	✓	$O(C/((1-\beta)T))$

2.3 Convergence Analysis

In general, the recommender system has some additional parameters $\theta \in \mathbb{R}^m$ except for embedding to be trained. Therefore, we analyze the convergence rate of the following gradient descent strategy:

$$\begin{aligned} \mathbf{E}_{t+1} &\leftarrow \mathbf{E}_t - \eta \hat{\psi}_{nsa}(\nabla_{\mathbf{E}} \mathcal{L}(\mathbf{E}_t, \theta_t)), \\ \theta_{t+1} &\leftarrow \theta_t - \eta' \nabla_{\theta} \mathcal{L}(\mathbf{E}_t, \theta_t). \end{aligned}$$

wherein SEvo is performed on the embedding and a normal gradient descent is applied to θ . To make the analysis feasible, some mild assumptions on the loss function should be given: $\mathcal{L} : \mathbb{R}^{n \times d} \times \mathbb{R}^m \rightarrow \mathbb{R}$ is a 2-times continuously differentiable function whose first derivative is Lipschitz continuous for some constant C . Then, we have the following properties.

THEOREM 2.2. *If $\eta = \eta' = 1/C$, after T updates, we have*

$$\min_{t \leq T} \|\nabla \mathcal{L}(\mathbf{E}_t, \theta_t)\|_2^2 = O(C/((1-\beta)^2T)).$$

If we adopt a modified learning rate for embedding:

$$\eta = \frac{1}{(1-\beta^{L+1})C},$$

the convergence rate could be improved to $O(C/((1-\beta)T))$.

REMARK 1. *Our main interest is to justify the designs of SEvo rather than to pursue a particular convergence rate, so some mild assumptions suggested in [31] are adopted here. By introducing the steepest descent for quadratic norms [1], better convergence can be obtained with stronger assumptions.*

Two conclusions can be drawn from Theorem 2.2. 1) The theoretical upper bound becomes worse when $\beta \rightarrow 1$. This makes sense since $\hat{\psi}_{nsa}(\nabla_{\mathbf{E}} \mathcal{L})$ is getting smoother and further away from the original descent direction. 2) A modified learning rate for embedding can significantly improve the convergence rate. This phenomenon can be understood readily if we notice the fact that

$$\|\hat{\psi}_{nsa}(\Delta \mathbf{E})\|_F \leq (1-\beta^{L+1})\|\Delta \mathbf{E}\|_F.$$

So the modified learning rate is indeed to offset the *scaling effect* resulted from SEvo. In view of this, we directly integrate this factor into SEvo to avoid getting stuck in the learning rate search, yielding the final desired transformation:

$$\hat{\psi}(\Delta \mathbf{E}; \beta) = \frac{1-\beta}{1-\beta^{L+1}} \sum_{l=0}^L \beta^l \tilde{\mathbf{A}}^l \Delta \mathbf{E}. \quad (7)$$

It can be shown that $\hat{\psi}$ is structure-aware and direction-aware, and still converges to ψ when L increases.

2.4 Pairwise Similarity Estimation

The previous discussion lays the technical basis for injecting graph structure information, but the final recommendation performance is determined by how ‘accurate’ the similarity estimation is. Following other GNN-based sequence models [45, 46], the number of consecutive occurrences across all sequences will be used as the pairwise similarity w_{ij} . In other words, items v_i and v_j that appear consecutively more often are assumed more related. Notably, we would like to emphasize that SEvo can readily inject other types of knowledge in addition to interaction data. For example, SEvo can be utilized to promote proximity among movie embeddings of the same genre, and to encourage a light-weight student model to mimic the embedding representations of a complex teacher model (i.e., knowledge distillation [17, 20]). We have made some preliminary efforts in Appendix D and observed some promising results.

2.5 Time Complexity

The time complexity of SEvo is mainly determined by the arithmetic operations of $\tilde{\mathbf{A}}^l \Delta \mathbf{E}$, $l = 1, 2, \dots, L$. Assuming that the number of non-zero entries of $\tilde{\mathbf{A}}$ is S , the complexity required is about $O(LsD)$. Because the recommendation datasets are known for high sparsity (i.e., S is very small), the actual computational overhead can be reduced to a very low level, almost negligible (see Section 4.2 for an empirical verification).

3 INTEGRATING SEVO INTO EXISTING OPTIMIZERS

Algorithm 1: SEvo-enhanced AdamW. Differences from the original AdamW are colored in blue. The matrix operation below are element-wise.

Input: embedding matrix \mathbf{E} , learning rate η , momentum factors β_1, β_2 , $\beta \in [0, 1)$, weight decay λ .

foreach step t **do**

$\mathbf{G}_t \leftarrow \nabla_{\mathbf{E}} \mathcal{L}$; // Get gradients w.r.t \mathbf{E}
 Update first/second moment estimates for each node i :

$$\mathbf{M}_t[i] \leftarrow \begin{cases} \beta_1 \mathbf{M}_{t-1}[i] + (1-\beta_1) \mathbf{G}_t[i] & \text{if } \mathbf{G}_t[i] \neq \mathbf{0} \\ \beta_1 \mathbf{M}_{t-1}[i] + \frac{(1-\beta_1)}{1-\beta_1^{t-1}} \mathbf{M}_{t-1}[i] & \text{otherwise} \end{cases},$$

$$\mathbf{V}_t[i] \leftarrow \begin{cases} \beta_2 \mathbf{V}_{t-1}[i] + (1-\beta_2) \mathbf{G}_t^2[i] & \text{if } \mathbf{G}_t[i] \neq \mathbf{0} \\ \beta_2 \mathbf{V}_{t-1}[i] + \frac{(1-\beta_2)}{1-\beta_2^{t-1}} \mathbf{V}_{t-1}[i] & \text{otherwise} \end{cases};$$

Compute bias-corrected first/second moment estimates:

$$\hat{\mathbf{M}}_t \leftarrow \mathbf{M}_t / (1-\beta_1^t), \quad \hat{\mathbf{V}}_t \leftarrow \mathbf{V}_t / (1-\beta_2^t);$$

Update via SEvo:

$$\mathbf{E}_t \leftarrow \mathbf{E}_{t-1} - \eta \hat{\psi} \left(\hat{\mathbf{M}}_t / \sqrt{\hat{\mathbf{V}}_t + \epsilon}; \beta \right) - \eta \lambda \mathbf{E}_{t-1}.$$

Output: optimized embeddings \mathbf{E} .

SEvo can be seamlessly integrated into existing optimizers since the variation involved in Eq. (2) can be extended beyond the (anti-)gradient. For SGD with momentum, the variation becomes the first moment estimate, and for Adam, this is jointly determined by

the first/second moment estimates. AdamW is also widely adopted for training recommenders. Unlike Adam whose moment estimate is a mixture of gradient and weight decay, AdamW decouples the weight decay from the optimization step, which is preferable since it makes no sense to require the weight decay to be smooth as well. However, in very rare cases (see Section 4.5), SEvo-enhanced AdamW fails to work very well. We next try to ascertain the causes and then propose a modification to make SEvo-enhanced AdamW more robust.

Denoted by $\mathbf{g} := \nabla_{\mathbf{e}} \mathcal{L} \in \mathbb{R}^d$ the gradient for a node embedding \mathbf{e} and $\mathbf{g}^2 := \mathbf{g} \odot \mathbf{g}$ the element-wise square, AdamW estimates the first and second moments at step t by the following formulas

$$\begin{aligned} \mathbf{m}_t &= \beta_1 \mathbf{m}_{t-1} + (1 - \beta_1) \mathbf{g}_{t-1}, \\ \mathbf{v}_t &= \beta_2 \mathbf{v}_{t-1} + (1 - \beta_2) \mathbf{g}_{t-1}^2, \end{aligned}$$

where β_1, β_2 are two momentum factors. Then the original AdamW updates each embedding vector as follows

$$\mathbf{e}_t = \mathbf{e}_{t-1} - \eta \cdot \Delta \mathbf{e}_{t-1}, \quad \Delta \mathbf{e}_{t-1} := \hat{\mathbf{m}}_t / \sqrt{\hat{\mathbf{v}}_t}.$$

Note that the bias-corrected estimates $\hat{\mathbf{m}}_t = \mathbf{m}_t / (1 - \beta_1^t)$ and $\hat{\mathbf{v}}_t = \mathbf{v}_t / (1 - \beta_2^t)$ are employed for numerical stability [22]. In practice, only a fraction of nodes will be sampled for training in a mini-batch, so the remaining embeddings have zero gradients. In this case, the sparse gradient problem may cause some unexpected ‘biases’.

PROPOSITION 3.1. *If a node is no longer sampled in subsequent p batches after step t , we have*

$$\Delta \mathbf{e}_{t+p-1} = \kappa \cdot \frac{\beta_1^p}{\sqrt{\beta_2^p}} \Delta \mathbf{e}_{t-1}, \quad (8)$$

where the coefficient of κ is mainly determined by t .

For a common case $\beta_2 \approx \beta_1$, the right-hand side of Eq. (8) is close to $\mathcal{O}(\beta_1^{p/2})$. The step size for inactive nodes then gets slower and slower during idle periods. This appears reasonable as their moment estimates are becoming outdated; however, this effect sometimes prevents the variation from being smoothed by SEvo. We hypothesize that this is because SEvo itself tends to assign more energy to active nodes and less energy to inactive nodes. So the effect of Eq. (8) is somewhat redundant. Fortunately, there is a feasible modification to make SEvo-enhanced AdamW more robust:

THEOREM 3.2. *Under the same assumptions as in Proposition 3.1, $\Delta \mathbf{e}_{t+p-1} = \Delta \mathbf{e}_{t-1}$ if the moment estimates are updated in the following manner when $\mathbf{g}_t = \mathbf{0}$,*

$$\mathbf{m}_t = \beta_1 \mathbf{m}_{t-1} + (1 - \beta_1) \frac{1}{1 - \beta_1^{t-1}} \mathbf{m}_{t-1}, \quad (9)$$

$$\mathbf{v}_t = \beta_2 \mathbf{v}_{t-1} + (1 - \beta_2) \frac{1}{1 - \beta_2^{t-1}} \mathbf{v}_{t-1}. \quad (10)$$

As can be seen, when sparse gradients are encountered, the approach in Theorem 3.2 is actually to estimate the current gradient from previous moments. The coefficients $1/(1 - \beta_1^{t-1})$ and $1/(1 - \beta_2^{t-1})$ are used here for unbiasedness (refer to Appendix A.3 for detailed discussion and proofs). We summarize SEvo-enhanced AdamW in Algorithm 1, and the algorithms for SGD and Adam can be found in Appendix B.

Table 2: Dataset statistics

Dataset	#Users	#Items	#Interactions	Density	Avg. Length
Beauty	22,363	12,101	198,502	0.07%	8.9
Toys	19,412	11,924	167,597	0.07%	8.6
Tools	16,638	10,217	134,476	0.08%	8.1
MovieLens-1M	6,040	3,416	999,611	4.84%	165.5

4 EXPERIMENTS

In this section, we comprehensively verify the superiority of SEvo. We focus on sequential recommendation for two reasons: 1) This is the most common scenario in practice; 2) Utilizing both sequence and structure information is beneficial yet challenging. We show-case that SEvo is a promising way to achieve this goal. Firstly, overall performance and efficiency comparisons are reported in Section 4.2. The empirical results in Section 4.3 then verify previous statements, showing both convergence and smoothness performance throughout training. An exhaustive ablation study will be given in Section 4.4. We also validate in Section 4.5 the correction of SEvo-enhanced AdamW. Due to space constraints, we defer the application of SEvo besides interaction data in Appendix D.

4.1 Experimental Setup

This part introduces the datasets, evaluation metrics, baselines, and implementation details.

Datasets. Four benchmark datasets, including Beauty, Toys, Tools, and MovieLens-1M, are considered in this paper. The first three are e-commerce datasets from Amazon reviews known for high sparsity, and MovieLens-1M is a movie dataset with a much longer sequence length. Following [12, 21], we filter out users and items with less than 5 interactions, and the validation set and test set are split in a *leave-one-out* fashion, namely the last interaction for testing and the penultimate one for validation. This splitting allows for fair comparisons, either for sequential recommendation or collaborative filtering. The dataset statistics are presented in Table 2.

Evaluation metrics. For each user, the predicted scores over *all items* will be sorted in descending order to generate top-N candidate lists. We consider two widely-used evaluation metrics, HR@N (Hit Rate) and NDCG@N (Normalized Discounted Cumulative Gain). The former measures the rate of successful hits among the top-N recommended candidates, while the latter takes into account the ranking positions and assigns higher scores in order of priority.

Baselines. We select four GNN-based models (**LightGCN** [15], **SR-GNN** [45], **LESSR** [7], and **MAERec** [48]) as performance and efficiency benchmarks, and four sequence models (**GRU4Rec** [16], **SASRec** [21], **BERT4Rec** [38], and **STOSA** [12]) as the backbones to validate the effectiveness of SEvo. Besides, **MF-BPR** [33] is also considered here as a backbone without sequence modeling. We carefully tune the hyperparameters according to their open-source code and experimental settings.

Implementation details. Since the purpose is to study the effectiveness of SEvo, only hyperparameters concerning optimization are returned, including learning rate, weight decay and dropout rate. Other hyperparameters in terms of the architecture are consistent with the corresponding baseline. For a fair comparison, the number

Table 3: Overall performance comparison. The best baselines and ours are marked in underline and **bold, respectively. Symbol $\blacktriangle\%$ stands for the relative gap between them. Paired t-test is performed over 5 independent runs for evaluating p -value (≤ 0.05 indicates statistical significance). ‘Avg. Improv.’ for each backbone depicts average relative improvements against the baseline.**

	GNN-based				MF or RNN/Transformer-based										$\blacktriangle\%$	p -value	
	LightGCN	SR-GNN	LESSR	MAERec	MF-BPR +SEvo	GRU4Rec +SEvo	SASRec +SEvo	BERT4Rec +SEvo	STOSA +SEvo								
Beauty	HR@1	0.0074	0.0059	0.0088	0.0113	0.0071	0.0076	0.0061	0.0094	0.0120	0.0154	0.0157	0.0172	<u>0.0166</u>	0.0216	30.2%	6.90E-05
	HR@5	0.0289	0.0247	0.0322	0.0424	0.0272	0.0293	0.0233	0.0326	0.0404	0.0499	<u>0.0479</u>	0.0522	<u>0.0479</u>	0.0544	13.5%	7.69E-04
	HR@10	0.0472	0.0406	0.0506	0.0662	0.0454	0.0480	0.0395	0.0524	0.0634	0.0759	<u>0.0716</u>	0.0772	<u>0.0680</u>	0.0774	8.2%	2.66E-03
	NDCG@5	0.0181	0.0152	0.0205	0.0269	0.0170	0.0184	0.0146	0.0209	0.0262	0.0328	0.0319	0.0350	<u>0.0327</u>	0.0383	17.2%	9.70E-05
	NDCG@10	0.0240	0.0203	0.0264	0.0346	0.0228	0.0244	0.0198	0.0273	0.0336	0.0411	<u>0.0395</u>	0.0430	<u>0.0391</u>	0.0457	15.5%	8.02E-05
Toys	HR@1	0.0087	0.0100	0.0126	0.0171	0.0079	0.0099	0.0059	0.0080	0.0172	0.0192	0.0160	0.0175	<u>0.0232</u>	0.0267	15.3%	1.46E-03
	HR@5	0.0279	0.0294	0.0352	0.0532	0.0267	0.0306	0.0209	0.0276	0.0506	0.0584	0.0430	0.0492	<u>0.0571</u>	0.0625	9.6%	5.70E-03
	HR@10	0.0456	0.0439	0.0513	<u>0.0796</u>	0.0427	0.0477	0.0345	0.0446	0.0727	0.0844	0.0645	0.0723	<u>0.0776</u>	0.0872	9.5%	3.07E-04
	NDCG@5	0.0183	0.0198	0.0240	<u>0.0355</u>	0.0174	0.0203	0.0134	0.0179	0.0342	0.0392	0.0297	0.0336	<u>0.0406</u>	0.0453	11.6%	2.48E-03
	NDCG@10	0.0240	0.0245	0.0292	0.0440	0.0225	0.0258	0.0177	0.0234	0.0413	0.0475	0.0366	0.0410	<u>0.0472</u>	0.0532	12.7%	3.12E-05
Tools	HR@1	0.0067	0.0046	0.0045	0.0083	0.0058	0.0071	0.0053	0.0058	<u>0.0099</u>	0.0108	0.0074	0.0087	0.0095	0.0133	33.8%	1.23E-02
	HR@5	0.0212	0.0162	0.0157	0.0271	0.0187	0.0225	0.0174	0.0208	<u>0.0317</u>	0.0337	0.0244	0.0279	0.0276	0.0350	10.5%	8.94E-03
	HR@10	0.0326	0.0260	0.0263	0.0423	0.0293	0.0348	0.0272	0.0336	<u>0.0466</u>	0.0497	0.0405	0.0441	0.0417	0.0502	7.7%	8.25E-03
	NDCG@5	0.0140	0.0103	0.0101	0.0177	0.0123	0.0147	0.0114	0.0133	<u>0.0210</u>	0.0223	0.0159	0.0183	0.0186	0.0244	15.9%	5.57E-03
	NDCG@10	0.0176	0.0135	0.0135	0.0226	0.0157	0.0187	0.0145	0.0174	<u>0.0258</u>	0.0274	0.0211	0.0235	0.0231	0.0293	13.4%	3.79E-03
MovieLens	HR@1	0.0124	0.0383	0.0513	0.0439	0.0117	0.0133	0.0487	0.0487	0.0490	0.0517	<u>0.0681</u>	0.0733	0.0457	0.0510	7.6%	3.81E-02
	HR@5	0.0495	0.1297	0.1665	0.1563	0.0470	0.0509	0.1625	0.1663	0.1599	0.1670	<u>0.2069</u>	0.2127	0.1409	0.1569	2.8%	4.17E-03
	HR@10	0.0866	0.2009	0.2539	0.2462	0.0836	0.0876	0.2522	0.2568	0.2492	0.2567	<u>0.3018</u>	0.3075	0.2185	0.2356	1.9%	9.32E-02
	NDCG@5	0.0307	0.0842	0.1092	0.1003	0.0291	0.0319	0.1061	0.1075	0.1046	0.1096	<u>0.1387</u>	0.1437	0.0932	0.1041	3.6%	4.19E-04
	NDCG@10	0.0427	0.1071	0.1373	0.1292	0.0408	0.0436	0.1350	0.1366	0.1333	0.1385	<u>0.1693</u>	0.1743	0.1181	0.1295	2.9%	1.30E-02
Avg. Improv.					+13.1%		+23.4%		+12.3%		+9.6%		+17.5%				

Table 4: Training and inference efficiency comparisons. The wall time (seconds) is evaluated on an Intel Xeon E5- 2620 v4 platform and a single GTX 1080Ti GPU. The number within parentheses indicates the additional time required for SEvo enhancement.

	Beauty		MovieLens-1M	
	Training	Inference	Training	Inference
LightGCN	2,000	1.07	6,898	1.95
SR-GNN	25,838	14.52	126,130	6.16
LESSR	19,687	14.35	203,226	5.02
MAERec	23,956	3.60	42,587	2.41
MF-BPR (+SEvo)	1,781 (+156)	0.96 (+0)	6,837 (+291)	1.95 (+0)
GRU4Rec (+SEvo)	928 (+59)	1.98 (+0)	12,116 (+271)	1.78 (+0)
SASRec (+SEvo)	446 (+24)	2.16 (+0)	919 (+35)	1.24 (+0)
BERT4Rec (+SEvo)	1,471 (+495)	2.03 (+0)	1,132 (+111)	1.18 (+0)
STOSA (+SEvo)	2,254 (+238)	9.84 (+0)	2,220 (+39)	1.98 (+0)

of layers L is fixed to 3 as in other GNN-based recommenders. As for the hyperparameter in terms of the degree of smoothness, we found $\beta = 0.99$ performs quite well in practice. The loss functions follow the suggestions in the respective papers, given that SEvo can be applied to any of them.

4.2 Overall Comparison

In this section, we are to verify the effectiveness of SEvo in boosting recommendation performance. Table 3 and Table 4 respectively compare the overall performance and efficiency over four public datasets, from which we have the following key observations:

- GNN-based models seem to over-emphasize structure information but lack full exploitation of sequence information. Their performance is only on par with GRU4Rec, a simple RNN with only one GRU layer. On the Tools dataset, SR-GNN and LESSR are even inferior to LightGCN, a collaborative filtering model with no access to sequence information. MAERec makes a slightly better attempt to combine the two by learning structure information through graph-based reconstruction tasks. It employs a SASRec backbone for recommendation to allow for a better utilization of sequence information. However, either dynamic graph construction in SR-GNN and LESSR, or path sampling in MAERec, requires heavy computational overhead (see Table 4). Particularly for SR-GNN and LESSR, these expensive costs are inevitable in both training and inference. Thus, previous efforts in mining graph structure information probably conflict with sequence information and are difficult to scale.
- Due to Transformer’s impressive capability in sequence encoding, SASRec, BERT4Rec and STOSA all achieve superior performance compared to GNN-based counterparts. As evident from the last two columns of Table 3, structure information learned through SEvo remains instrumental even for state-of-the-art methods, providing consistent performance gains of 2% to 30%. Moreover, SASRec trained with SEvo-enhanced AdamW has outperformed MAERec despite their identical recommendation backbones. Note that SEvo does not change the inference logic of the model, so the inference time remains unchanged. Besides, the computational overhead required in training is also negligible compared to previous graph-enhanced models that employ GNNs as intermediate modules. SEvo is arguably superior to these cumbersome GNN modules in real-world applications. Not to mention that the non-sequential approach MF-BPR can also benefit from SEvo and

achieves comparable performance to LightGCN, demonstrating the universality of SEvo. Overall, the significant improvements from the SEvo enhancement suggest a promising route to exploit graph structure information, especially in conjunction with sequence modeling.

Since SASRec is a pioneer in the field of sequential recommendation, it will serve as the default backbone for subsequent studies.

4.3 Empirical Analysis

Convergence comparison. In Section 2.3, we theoretically verified the necessity of rescaling the original Neumann series approximation for faster convergence. Figure 2a shows the loss curves of SASRec trained with AdamW using identical settings other than the form of SEvo. Without rescaling, SASRec exhibits significantly slower convergence, consistent with the conclusion in Theorem 2.2. While the theoretical worst-case convergence rate of the corrected SEvo is only 1% of the normal gradient descent when $\beta = 0.99$, its practical performance is much better. SASRec trained with SEvo-enhanced AdamW initially converges marginally slower and catches up in the final stage.

Smoothness evaluation. Figure 2b demonstrates the variation’s smoothness throughout the evolution process and the eventual embedding differences from $\beta = 0$ to $\beta = 0.999$. **(I) \rightarrow (II):** The original variations are roughly as smooth, but after transformation, they are quite different—smoother as β increases. **(II) \rightarrow (III):** Consequently, the embedding trained with a stronger smoothness constraint becomes smoother as well. The structure-aware embedding evolution successfully makes related nodes closer in the latent space. Although smoothness is not the sole quality measure of embedding, combined with the analyses above, we can conclude that SEvo injects appropriate structure information under the default setting of $\beta = 0.99$.

4.4 Ablation Study

SEvo for various optimizers. It is of interest to study whether SEvo can be extended to other commonly used optimizers such as SGD and Adam. Figure 3a compares NDCG@10 performance on Beauty and MovieLens-1M. For a fair comparison, the hyperparameters are tuned independently. It is clear that the performance of SGD, Adam, and AdamW improves significantly after incorporating SEvo, with AdamW achieving the best as it does not need to smooth the weight decay.

Neumann series approximation versus iterative approximation. Theorem 2.1 suggests that the Neumann series approximation is preferable to the commonly used iterative approximation because the latter is not always direction-aware and thus a conservative hyperparameter of β is needed to ensure convergence. This conclusion can also be drawn from Figure 3b. When a little smoothness is required, their performance is comparable as both approximations differ only at the last term. The iterative approximation however fails to ensure convergence once $\beta > 0.7$ on Beauty and $\beta > 0.9$ on MovieLens-1M. This may result in a lack of smoothness.

L-layer Approximation. As L increases, SEvo gets closer to the exact solution while accessing higher-order neighborhood information. Table 5 lists the performance of different layers, which reaches

Table 5: SEvo using different approximation layers L .

	Beauty			MovieLens1M		
	HR@1	HR@10	NDCG@10	HR@1	HR@10	NDCG@10
$L=0$	0.0124	0.0664	0.0353	0.0465	0.2487	0.1321
$L=1$	0.0140	0.0717	0.0388	0.0498	0.2562	0.1372
$L=2$	0.0152	0.0740	0.0403	0.0511	0.2589	0.1389
$L=3$	0.0154	0.0759	0.0411	0.0517	0.2567	0.1385
$L=4$	0.0153	0.0755	0.0408	0.0510	0.2576	0.1383
$L=5$	0.0150	0.0750	0.0403	0.0492	0.2581	0.1382

its peak around $L = 3$ and starts to decrease then. A possible reason is that the higher-order information is over-smoothed and thus not as reliable and easy to use as the lower order information. Similar phenomena have been found in previous works [7, 47] on applying GNNs to recommendation.

4.5 Moment Estimate Correction for AdamW

We compare SEvo-enhanced AdamW with or without moment estimate correction in Figure 4, in which average relative improvements against the baseline are presented for each recommender. Overall, the two variants of SEvo-enhanced AdamW perform comparably, significantly surpassing the baseline. However, in some cases (e.g., GRU4Rec and STOSA), the moment estimate correction as suggested in Theorem 3.2 is particularly useful to improve performance. Recall that BERT4Rec is trained using the output softmax from a separate fully-connected layer that is fully updated at each step. This may explain why the correction has little effect on BERTRec. In conclusion, the results highlight the importance of the proposed modification in alleviating bias in moment estimates.

5 RELATED WORK

Recommender systems are developed to enable users to quickly and accurately find relevant items in diverse applications, such as e-commerce [53], online news [14] and social media [4]. Typically, the entities involved are embedded into a latent space [5, 11, 50], and then decision models are built on top of the embedding for tasks like collaborative filtering [15] and context/knowledge-aware recommendation [41, 43]. Sequential recommendation [24, 34] focuses on capturing users’ dynamic interests from their historical interaction sequences. Early approaches adapted recurrent neural networks (RNNs) [16] and convolutional filters [40] for sequence modeling. Recently, Transformer [10, 42] has become a popular architecture for sequence modeling due to its parallel efficiency and superior performance. SASRec [21] and BERT4Rec [38] use unidirectional and bidirectional self-attention, respectively. Fan et al. [12] proposed a novel stochastic self-attention (STOSA) to model the uncertainty of sequential behaviors.

Graph neural networks [2, 9] are a type of neural network designed to operate on graph-structured data, in concert with a weighted adjacency matrix to characterize the pairwise relations between nodes. GNN equipped with this adjacency matrix can be used for message passing between nodes. The most relevant work is the optimization framework proposed in [52] for solving semi-supervised learning problems via a smoothness constraint. This graph regularization approach has recently inspired a series

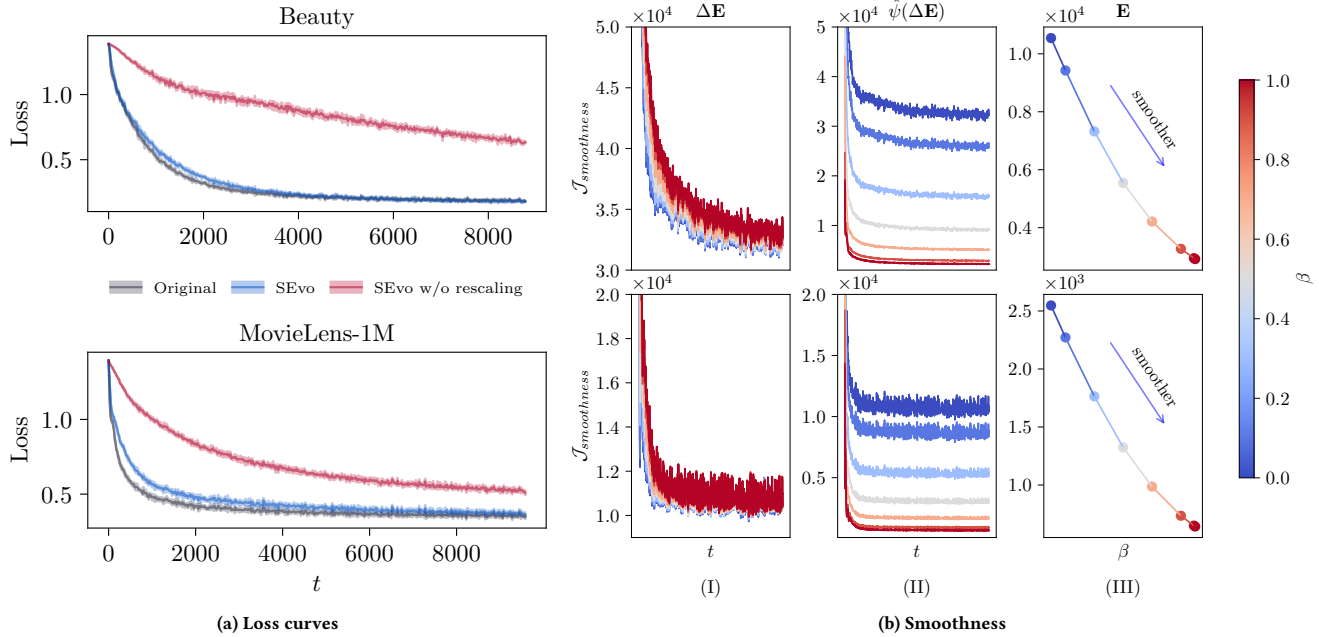


Figure 2: Empirical illustrations of convergence and smoothness. The top and bottom panels respectively depict the results for Beauty and MovieLens-1M. (a) SASRec enhanced by SEvo with or without rescaling. (b) Smoothness of (I) the original variation; (II) the smoothed variation; (III) the optimized embedding. A lower $\mathcal{J}_{smoothness}$ indicates stronger smoothness.

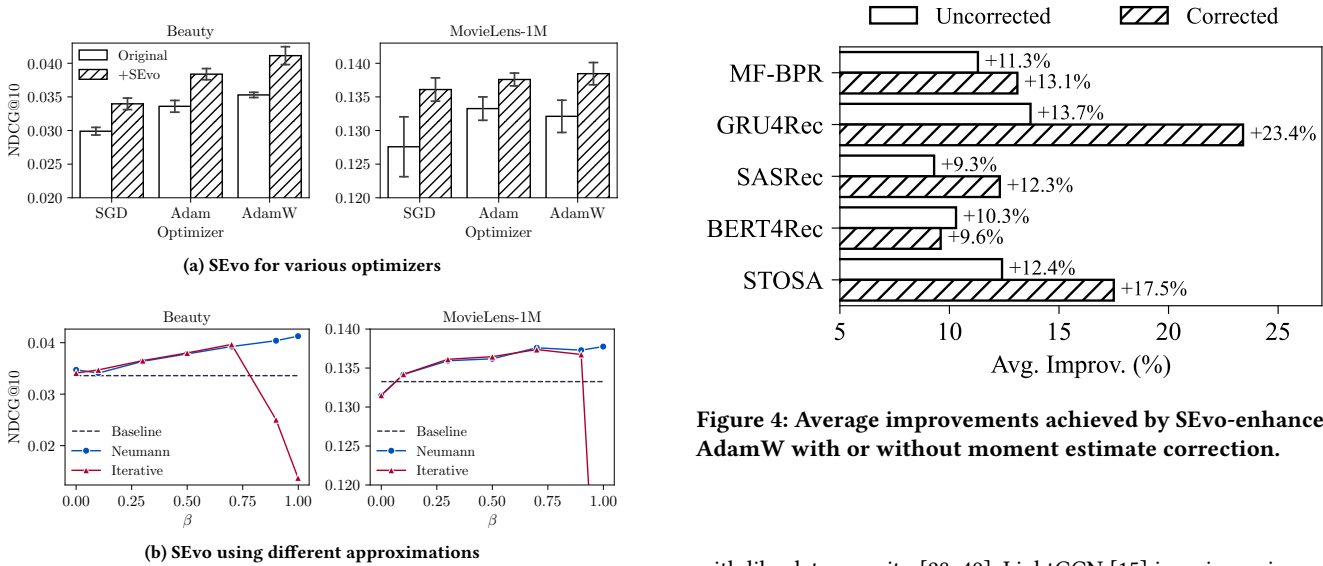


Figure 3: SEvo ablation experiments: (a) SEvo-enhanced SGD, Adam and AdamW; (b) Neumann series approximation versus iterative approximation.

of work [6, 27, 55]. As opposed to applying it to smooth node representations [23] or labels [18], it is employed here primarily to balance smoothness and convergence on the variation.

Structure information in recommendation is typically learned through GNN as well, with specific modifications made to cope

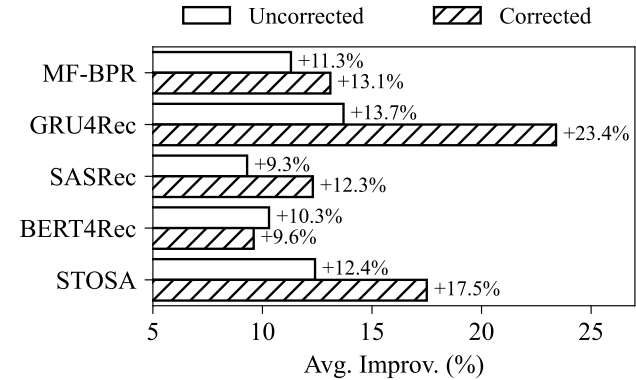


Figure 4: Average improvements achieved by SEvo-enhanced AdamW with or without moment estimate correction.

with like data sparsity [28, 49]. LightGCN [15] is a pioneering collaborative filtering work on modeling user-item relations, which removes nonlinearities for easier training. UltraGCN [28] develops a reweighted binary cross-entropy loss to approach the smoothness after stacking infinite layers. To further utilize sequence information, previous efforts focus on equipping sequence models with complex GNN modules, but this inevitably increases the computational cost of training and inference, making it unappealing for practical recommendation. For example, SR-GNN [45] and LESSR [7] need dynamically construct adjacency matrices for each batch of

sequences. Differently, MAERec [48] proposes an adaptive data augmentation to boost a novel graph masked autoencoder, which learns to sample less noisy paths from semantic similarity graph for subsequent reconstruction tasks. The resulting strong self-supervision signals help the model capture more useful information.

6 CONCLUSION

In this work, we have proposed a novel update mechanism for injecting graph structure information into embedding. Theoretical analyses of the convergence properties motivate some necessary modifications to the proposed method. SEvo can be seamlessly integrated into existing optimizers. For AdamW, we recorrect the moment estimates to make it more robust. The experimental results over four public datasets demonstrate the superiority.

An interesting direction for future work is extending SEvo to multiplex heterogeneous graphs [3], as real-world entities often participate in various relation networks. Furthermore, while directed graphs can be converted to undirected graphs, this operation inevitably results in loss of information. How to leverage this directional information remains an open challenge and another promising area for further investigation.

REFERENCES

- [1] Stephen P Boyd and Lieven Vandenberghe. 2004. *Convex optimization*. Cambridge university press.
- [2] Joan Bruna, Wojciech Zaremba, Arthur Szlam, and Yann LeCun. 2014. Spectral networks and locally connected networks on graphs. In *International Conference on Learning Representations (ICLR)*.
- [3] Yukuo Cen, Xu Zou, Jianwei Zhang, Hongxia Yang, Jingren Zhou, and Jie Tang. 2019. Representation learning for attributed multiplex heterogeneous network. In *ACM SIGKDD International Conference on Knowledge Discovery & Data Mining (KDD)*. 1358–1368.
- [4] Jiajia Chen, Xin Xin, Xianfeng Liang, Xiangnan He, and Jun Liu. 2022. GDSRec: Graph-based decentralized collaborative filtering for social recommendation. *IEEE Transactions on Knowledge and Data Engineering (TKDE)* (2022).
- [5] Qiwei Chen, Huan Zhao, Wei Li, Pipei Huang, and Wenwu Ou. 2019. Behavior sequence transformer for e-commerce recommendation in alibaba. In *Proceedings of the 1st International Workshop on Deep Learning Practice for High-dimensional Sparse Data*. 1–4.
- [6] Siheng Chen, Aliaksei Sandryhaila, José MF Moura, and Jelena Kovacevic. 2014. Signal denoising on graphs via graph filtering. In *IEEE Global Conference on Signal and Information Processing (GlobSIP)*. IEEE, 872–876.
- [7] Tianwen Chen and Raymond Chi-Wing Wong. 2020. Handling information loss of graph neural networks for session-based recommendation. In *ACM SIGKDD International Conference on Knowledge Discovery & Data Mining (KDD)*. 1172–1180.
- [8] Kyunghyun Cho, Bart van Merriënboer, Dzmitry Bahdanau, and Yoshua Bengio. 2014. On the properties of neural machine translation: Encoder-decoder approaches. In *Proceedings of SSST@EMNLP 2014, Eighth Workshop on Syntax, Semantics and Structure in Statistical Translation*. ACL, 103–111.
- [9] Michaël Defferrard, Xavier Bresson, and Pierre Vandergheynst. 2016. Convolutional neural networks on graphs with fast localized spectral filtering. In *Advances in Neural Information Processing Systems (NeurIPS)*, Vol. 29.
- [10] Jacob Devlin, Ming-Wei Chang, Kenton Lee, and Kristina Toutanova. 2019. BERT: Pre-training of deep bidirectional transformers for language understanding. In *Conference of the North American Chapter of the Association for Computational Linguistics: Human Language Technologies (NAACL-HLT)*. ACL, 4171–4186.
- [11] Ahmed El-Kishky, Thomas Markovich, Serim Park, Chetan Verma, Baekjin Kim, Ramy Eskander, Yury Malkov, Frank Portman, Sofia Samaniego, Ying Xiao, et al. 2022. Twihin: Embedding the twitter heterogeneous information network for personalized recommendation. In *ACM SIGKDD International Conference on Knowledge Discovery & Data Mining (KDD)*. 2842–2850.
- [12] Ziwei Fan, Zhiwei Liu, Yu Wang, Alice Wang, Zahra Nazari, Lei Zheng, Hao Peng, and Philip S Yu. 2022. Sequential recommendation via stochastic self-attention. In *ACM Web Conference (WWW)*. 2036–2047.
- [13] Justin Gilmer, Samuel S Schoenholz, Patrick F Riley, Oriol Vinyals, and George E Dahl. 2017. Neural message passing for quantum chemistry. In *International Conference on Machine Learning (ICML)*. PMLR, 1263–1272.
- [14] Shansan Gong and Kenny Q Zhu. 2022. Positive, negative and neutral: Modeling implicit feedback in session-based news recommendation. In *International ACM Conference on Research and Development in Information Retrieval (SIGIR)*.
- [15] Xiangnan He, Kuan Deng, Xiang Wang, Yan Li, Yongdong Zhang, and Meng Wang. 2020. Lightgcn: Simplifying and powering graph convolution network for recommendation. In *International ACM Conference on Research and Development in Information Retrieval (SIGIR)*. 639–648.
- [16] Balázs Hidasi, Alexandros Karatzoglou, Linas Baltrunas, and Domonkos Tikk. 2016. Session-based recommendations with recurrent neural networks. In *International Conference on Learning Representations (ICLR)*.
- [17] Geoffrey E. Hinton, Oriol Vinyals, and Jeffrey Dean. 2015. Distilling the knowledge in a neural network. *CoRR* abs/1503.02531 (2015).
- [18] Qian Huang, Horace He, Abhay Singh, Ser-Nam Lim, and Austin R. Benson. 2021. Combining label propagation and simple models out-performs graph neural networks. In *International Conference on Learning Representations (ICLR)*.
- [19] Tony Jebara, Jun Wang, and Shih-Fu Chang. 2009. Graph construction and b-matching for semi-supervised learning. In *International Conference on Machine Learning (ICML)*. 441–448.
- [20] SeongKu Kang, Junyoung Hwang, Wonbin Kweon, and Hwanjo Yu. 2021. Topology distillation for recommender system. In *ACM SIGKDD Conference on Knowledge Discovery and Data Mining*. ACM, 829–839.
- [21] Wang-Cheng Kang and Julian McAuley. 2018. Self-attentive sequential recommendation. In *IEEE International Conference on Data Mining (ICDM)*. IEEE, 197–206.
- [22] Diederik P. Kingma and Jimmy Ba. 2015. Adam: A method for stochastic optimization. In *International Conference on Learning Representations (ICLR)*.
- [23] Johannes Klicpera, Aleksandar Bojchevski, and Stephan Günnemann. 2019. Predict then propagate: Graph neural networks meet personalized pagerank. In *International Conference on Learning Representations (ICLR)*.
- [24] Jiacheng Li, Yujie Wang, and Julian McAuley. 2020. Time interval aware self-attention for sequential recommendation. In *International Conference on Web Search and Data Mining (WSDM)*. 322–330.
- [25] Qimai Li, Zhichao Han, and Xiao-Ming Wu. 2018. Deeper insights into graph convolutional networks for semi-supervised learning. In *Conference on Artificial Intelligence (AAAI)*.
- [26] Ilya Loshchilov and Frank Hutter. 2018. Decoupled weight decay regularization. In *International Conference on Learning Representations (ICLR)*.
- [27] Yao Ma, Xiaorui Liu, Tong Zhao, Yozen Liu, Jiliang Tang, and Neil Shah. 2021. A unified view on graph neural networks as graph signal denoising. In *ACM International Conference on Information and Knowledge Management (CIKM)*. 1202–1211.
- [28] Kelong Mao, Jieming Zhu, Xi Xiao, Biao Lu, Zhaowei Wang, and Xiuqiang He. 2021. UltraGCN: Ultra simplification of graph convolutional networks for recommendation. In *International Conference on Information and Knowledge Management (CIKM)*.
- [29] Leland McInnes, John Healy, and James Melville. 2018. Umap: Uniform manifold approximation and projection for dimension reduction. *arXiv preprint arXiv:1802.03426* (2018).
- [30] Miller McPherson, Lynn Smith-Lovin, and James M Cook. 2001. Birds of a feather: Homophily in social networks. *Annual Review of Sociology* (2001), 415–444.
- [31] Yurii Nesterov. 1998. Introductory lectures on convex programming volume i: Basic course. *Lecture notes* 3, 4 (1998), 5.
- [32] Wonpyo Park, Dongju Kim, Yan Lu, and Minsu Cho. 2019. Relational knowledge distillation. In *IEEE Conference on Computer Vision and Pattern Recognition (CVPR)*. IEEE, 3967–3976.
- [33] Steffen Rendle, Christoph Freudenthaler, Zeno Gantner, and Schmidt-Thieme Lars. 2009. BPR: Bayesian personalized ranking from implicit feedback. In *Conference on Uncertainty in Artificial Intelligence (UAI)*.
- [34] Guy Shani, David Heckerman, Ronen I Brafman, and Craig Boutilier. 2005. An MDP-based recommender system. *Journal of Machine Learning Research (JMLR)* 6, 9 (2005).
- [35] Kartik Sharma, Yeon-Chang Lee, Sivagami Nambi, Aditya Salian, Shlok Shah, Sang-Wook Kim, and Srijan Kumar. 2022. A survey of graph neural networks for social recommender systems. *arXiv preprint arXiv:2212.04481* (2022).
- [36] Daniel A Spielman. 2007. Spectral graph theory and its applications. In *Annual IEEE Symposium on Foundations of Computer Science (FOCS'07)*. IEEE, 29–38.
- [37] Gilbert W Stewart. 1998. *Matrix algorithms: volume 1: basic decompositions*. SIAM.
- [38] Fei Sun, Jun Liu, Jian Wu, Changhua Pei, Xiao Lin, Wenwu Ou, and Peng Jiang. 2019. BERT4Rec: Sequential recommendation with bidirectional encoder representations from transformer. In *ACM International Conference on Information and Knowledge Management (CIKM)*. 1441–1450.
- [39] Ilya Sutskever, James Martens, George Dahl, and Geoffrey Hinton. 2013. On the importance of initialization and momentum in deep learning. In *International Conference on Machine Learning (ICML)*. PMLR, 1139–1147.
- [40] Jiayi Tang and Ke Wang. 2018. Personalized top-n sequential recommendation via convolutional sequence embedding. In *ACM International Conference on Web Search and Data Mining (WSDM)*. ACM, 565–573.
- [41] Zhen Tian, Ting Bai, Wayne Xin Zhao, Ji-Rong Wen, and Zhao Cao. 2023. EulerNet: Adaptive feature interaction learning via Euler’s formula for CTR prediction. In *International ACM SIGIR Conference on Research and Development in Information Retrieval (SIGIR)*. ACM, 1376–1385.
- [42] Ashish Vaswani, Noam Shazeer, Niki Parmar, Jakob Uszkoreit, Llion Jones, Aidan N Gomez, Lukasz Kaiser, and Illia Polosukhin. 2017. Attention is all you need. In *Advances in Neural Information Processing Systems (NeurIPS)*, Vol. 30.
- [43] Xiang Wang, Xiangnan He, Yixin Cao, Meng Liu, and Tat-Seng Chua. 2019. Kgat: Knowledge graph attention network for recommendation. In *ACM SIGKDD International Conference on Knowledge Discovery & Data Mining (KDD)*. 950–958.
- [44] Yu Wang, Yuying Zhao, Yi Zhang, and Tyler Derr. 2023. Collaboration-aware graph convolutional network for recommender systems. In *ACM Web Conference (WWW)*. 91–101.
- [45] Shu Wu, Yuyuan Tang, Yanqiao Zhu, Liang Wang, Xing Xie, and Tieniu Tan. 2019. Session-based recommendation with graph neural networks. In *Conference on Artificial Intelligence (AAAI)*, Vol. 33. 346–353.
- [46] Xin Xia, Hongzhi Yin, Junliang Yu, Qinyong Wang, Lizhen Cui, and Xiangliang Zhang. 2021. Self-supervised hypergraph convolutional networks for session-based recommendation. In *Conference on Artificial Intelligence (AAAI)*, Vol. 35. 4503–4511.
- [47] Cong Xu, Jun Wang, and Wei Zhang. 2023. StableGCN: Decoupling and reconciling information propagation for collaborative filtering. *IEEE Transactions on Knowledge and Data Engineering (TKDE)* (2023).
- [48] Yaowen Ye, Lianghao Xia, and Chao Huang. 2023. Graph masked autoencoder for sequential recommendation. In *International ACM Conference on Research and Development in Information Retrieval (SIGIR)*. ACM, 321–330.
- [49] Rex Ying, Ruining He, Kaifeng Chen, Pong Eksombatchai, William L Hamilton, and Jure Leskovec. 2018. Graph convolutional neural networks for web-scale recommender systems. In *ACM SIGKDD International Conference on Knowledge Discovery & Data Mining (KDD)*. 974–983.
- [50] Shengyu Zhang, Fuli Feng, Kun Kuang, Wenqiao Zhang, Zhou Zhao, Hongxia Yang, Tat-Seng Chua, and Fei Wu. 2023. Personalized latent structure learning for

recommendation. *IEEE Transactions on Pattern Analysis and Machine Intelligence (TPAMI)* (2023).

- [51] Borui Zhao, Quan Cui, Renjie Song, Yiyu Qiu, and Jiajun Liang. 2022. Decoupled knowledge distillation. In *IEEE Conference on Computer Vision and Pattern Recognition (CVPR)*. IEEE, 11943–11952.
- [52] Dengyong Zhou, Olivier Bousquet, Thomas Lal, Jason Weston, and Bernhard Schölkopf. 2003. Learning with local and global consistency. *Advances in Neural Information Processing Systems (NeurIPS)* 16 (2003).
- [53] Guorui Zhou, Xiaoqiang Zhu, Chenru Song, Ying Fan, Han Zhu, Xiao Ma, Yanghui Yan, Junqi Jin, Han Li, and Kun Gai. 2018. Deep interest network for click-through rate prediction. In *ACM SIGKDD International Conference on Knowledge Discovery & Data Mining (KDD)*. 1059–1068.
- [54] Jiong Zhu, Yujun Yan, Lingxiao Zhao, Mark Heimann, Leman Akoglu, and Danai Koutra. 2020. Beyond homophily in graph neural networks: Current limitations and effective designs. 33 (2020), 7793–7804.
- [55] Meiqi Zhu, Xiao Wang, Chuan Shi, Houye Ji, and Peng Cui. 2021. Interpreting and unifying graph neural networks with an optimization framework. In *ACM Web Conference (WWW)*. 1215–1226.

CONTENTS

Abstract	1
1 Introduction	1
2 Structure-aware Embedding Evolution	2
2.1 Preliminaries	2
2.2 Methodology	3
2.3 Convergence Analysis	4
2.4 Pairwise Similarity Estimation	4
2.5 Time Complexity	4
3 Integrating SEvo into Existing Optimizers	4
4 Experiments	5
4.1 Experimental Setup	5
4.2 Overall Comparison	6
4.3 Empirical Analysis	7
4.4 Ablation Study	7
4.5 Moment Estimate Correction for AdamW	7
5 Related Work	7
6 Conclusion	9
References	10
Contents	11
A Proofs	11
A.1 Structure/Direction-aware Transformation	11
A.2 Convergence Analysis	13
A.3 Proofs of SEvo-enhanced AdamW	14
B Algorithms	15
C Baselines	15
D Pairwise Similarity Estimation	16
D.1 SEvo for Interaction Data	16
D.2 SEvo for Node Categories	17
D.3 SEvo for Knowledge Distillation	17
E Additional Experimental Results	18

A PROOFS

A.1 Structure/Direction-aware Transformation

In this part, we are to prove the structure-aware/direction-aware properties of the L -layer iterative approximation [52]:

$$\begin{aligned}\hat{\psi}_{iter}(\Delta E) &:= \hat{\psi}_L(\Delta E) \\ &= \underbrace{\left\{ (1-\beta) \sum_{l=0}^{L-1} \beta^l \tilde{\mathbf{A}}^l + \beta^L \tilde{\mathbf{A}}^L \right\}}_{=: \mathbf{P}'} \Delta E,\end{aligned}\quad (11)$$

and the L -layer Neumann series approximation [37]:

$$\hat{\psi}_{nsa}(\Delta E) = \underbrace{(1-\beta) \sum_{l=0}^L \beta^l \tilde{\mathbf{A}}^l}_{=: \mathbf{P}} \Delta E. \quad (12)$$

FACT 1. *If L is odd, the geometric series $S(x) = \sum_{k=0}^L x^k$ is monotonically increasing when $x \leq 0$.*

PROOF. It is easy to show that

$$S(x) = \frac{1 - x^{L+1}}{1 - x},$$

and the derivative w.r.t $x \neq 1$ is

$$S'(x) = \frac{Lx^{L+1} - (L+1)x^L + 1}{(1-x)^2}.$$

If L is odd, $S'(x)$ is positive when $x \leq 0$ and in this case $S(x)$ is monotonically increasing. \square

LEMMA A.1. *Given a normalized adjacency matrix $\tilde{\mathbf{A}} \in \mathbb{R}^{n \times n}$, let the symmetric matrix deduced from the Neumann series approximation be*

$$\mathbf{P} = (1-\beta) \sum_{l=0}^L \beta^l \tilde{\mathbf{A}}^l. \quad (13)$$

Denoted by $\lambda_{\min}(\mathbf{P})$, $\lambda_{\max}(\mathbf{P})$ the smallest and largest eigenvalues of \mathbf{P} , respectively, then we have $\forall \beta \in [0, 1)$

$$\frac{1-\beta}{1+\beta} (1-\beta^L) \leq \lambda_{\min}(\mathbf{P}) \leq \lambda_{\max}(\mathbf{P}) = 1 - \beta^{L+1}. \quad (14)$$

PROOF. It is easy to shown that the eigenvalues of \mathbf{P} are in the form of

$$\tilde{\lambda}_i = (1-\beta) \sum_{l=0}^L \beta^l \lambda_i^l, \quad i = 1, 2, \dots, n, \quad (15)$$

where $\lambda_1 \leq \lambda_2 \leq \dots \leq \lambda_n$ denote the eigenvalues of $\tilde{\mathbf{A}}$. Recall that these eigenvalues all fall into $[-1, 1]$ and $\lambda_n = 1$ can be achieved exactly [36]. Hence,

$$\tilde{\lambda}_n = (1-\beta) \sum_{l=0}^L \beta^l = 1 - \beta^{L+1} \quad (16)$$

is the largest eigenvalue of \mathbf{P} .

In addition, notice that the last term $(1-\beta)\beta^L\lambda^L$ is non-negative when L is even. Then, we can get a lower bound no matter L is odd or even:

$$\tilde{\lambda} = (1-\beta) \sum_{l=0}^L \beta^l \lambda^l \geq (1-\beta) \underbrace{\sum_{l=0}^{2\lfloor(L-1)/2\rfloor+1} \beta^l \lambda^l}_{=:S(\lambda)}. \quad (17)$$

The minimum of $S(\lambda)$ must be achieved in $[-1, 0]$ because $S(-\lambda) \leq S(\lambda)$ for any $\lambda > 0$. In fact, in view of Fact 1, we know that $S(\lambda) \geq S(-1)$. Hence, we have

$$\begin{aligned} \tilde{\lambda} &\geq (1-\beta)S(-1) = (1-\beta) \sum_{l=0}^{2\lfloor(L-1)/2\rfloor+1} \beta^l (-1)^l \\ &= (1-\beta) \sum_{l=0}^{\lfloor(L-1)/2\rfloor} (\beta^{2l} - \beta^{2l+1}) \\ &= (1-\beta)^2 \sum_{l=0}^{\lfloor(L-1)/2\rfloor} \beta^{2l} = (1-\beta)^2 \frac{(1-\beta^{2\lfloor(L-1)/2\rfloor+2})}{1-\beta^2} \\ &= \frac{1-\beta}{1+\beta} (1-\beta^{2\lfloor(L-1)/2\rfloor+2}) \geq \frac{1-\beta}{1+\beta} (1-\beta^L). \end{aligned} \quad (18)$$

The last inequality holds because $2\lfloor(L-1)/2\rfloor+2 \geq L$. Therefore, the smallest eigenvalue of \mathbf{P} must be greater than

$$\frac{1-\beta}{1+\beta} (1-\beta^L).$$

□

PROPOSITION A.2. *The Neumann series approximation is structure-aware and direction-aware for any $\beta \in [0, 1)$.*

PROOF. In view of Lemma A.1, we know

$$\lambda_{\min}(\mathbf{P}) \geq \frac{1-\beta}{1+\beta} (1-\beta^L) > 0, \quad \forall \beta \in [0, 1),$$

so \mathbf{P} is positive definite and thus $\hat{\psi}_{nsa}(\cdot)$ is direction-aware. Also, notice that \mathbf{P} has the same eigenvectors as $\tilde{\mathbf{A}}$, and so does $\tilde{\mathbf{L}}$. Hence, it is also structure-aware:

$$\begin{aligned} \langle \hat{\psi}_{nsa}(\mathbf{x}), \tilde{\mathbf{L}}\hat{\psi}_{nsa}(\mathbf{x}) \rangle &= \langle \hat{\psi}_{nsa}(\mathbf{x}), \tilde{\mathbf{L}}\hat{\psi}_{nsa}(\mathbf{x}) \rangle = \langle \mathbf{P}\mathbf{x}, \tilde{\mathbf{L}}\mathbf{P}\mathbf{x} \rangle \\ &= \langle \mathbf{x}, \mathbf{P}^T \tilde{\mathbf{L}}\mathbf{P}\mathbf{x} \rangle \leq \langle \mathbf{x}, \tilde{\mathbf{L}}\mathbf{x} \rangle. \end{aligned}$$

The last inequality follows from the fact $\lambda_{\max}(\mathbf{P}) \leq 1$.

□

LEMMA A.3. *Given a normalized adjacency matrix $\tilde{\mathbf{A}} \in \mathbb{R}^{n \times n}$, let the symmetric matrix deduced from the iterative approximation be*

$$\mathbf{P}' = (1-\beta) \sum_{l=0}^{L-1} \beta^l \tilde{\mathbf{A}}^l + \beta^L \tilde{\mathbf{A}}^L. \quad (19)$$

We have $\lambda_{\min}(\mathbf{P}') > 0, \forall \beta < 1/2$.

PROOF. This conclusion is trivial for the case of $L \leq 1$. Let us assume that $L \geq 2$. Firstly, rewrite Eq. (19) as

$$\mathbf{P}' = \mathbf{P} + \beta^L \tilde{\mathbf{A}}^L, \quad (20)$$

where $\mathbf{P} := (1-\beta) \sum_{l=0}^{L-1} \beta^l \tilde{\mathbf{A}}^l$. \mathbf{P} is positive definite in view of Lemma A.1 and $\beta^L \tilde{\mathbf{A}}^L$ is positive semidefinite when L is even. Therefore, only the case of $L \geq 3$ needs to be proved. For a vector \mathbf{x} , we have

$$\begin{aligned} \mathbf{x}^T \mathbf{P}' \mathbf{x} &= \mathbf{x}^T \mathbf{P} \mathbf{x} + \beta^L \mathbf{x}^T \tilde{\mathbf{A}}^L \mathbf{x} \\ &\geq \lambda_{\min}(\mathbf{P}) \|\mathbf{x}\|_2^2 + \beta^L \lambda_{\min}(\tilde{\mathbf{A}})^L \|\mathbf{x}\|_2^2 \end{aligned} \quad (21)$$

$$\geq \left(\frac{1-\beta}{1+\beta} (1-\beta^{L-1}) + \beta^L \lambda_{\min}(\tilde{\mathbf{A}})^L \right) \|\mathbf{x}\|_2^2 \quad (22)$$

$$\geq \left(\frac{1-\beta}{1+\beta} (1-\beta^{L-1}) - \beta^L \right) \|\mathbf{x}\|_2^2$$

$$= \frac{1-\beta-\beta^{L-1}-\beta^{L+1}}{1+\beta} \|\mathbf{x}\|_2^2$$

$$\geq \frac{1-\beta-\beta^2-\beta^4}{1+\beta} \|\mathbf{x}\|_2^2. \quad (23)$$

The first two inequalities follow from Lemma A.1. The last inequality holds by noting the fact that, for $L \geq 3$ and $\beta < 1/2$,

$$\beta + \beta^{L-1} + \beta^{L+1} \leq \beta + \beta^2 + \beta^4 < 13/16.$$

Therefore,

$$\lambda_{\min}(\mathbf{P}') = \min_{\mathbf{x}} \frac{\mathbf{x}^T \mathbf{P}' \mathbf{x}}{\|\mathbf{x}\|^2} \geq \frac{1-\beta-\beta^2-\beta^4}{1+\beta} > 0. \quad (24)$$

□

PROPOSITION A.4. *The iterative approximation is direction-aware for all possible normalized adjacency matrices and $L \geq 0$, if and only if $\beta < 1/2$.*

PROOF. If $\beta < 1/2$, we have $\lambda_{\min}(\mathbf{P}') > 0$ according to Lemma A.3, and thus $\hat{\psi}$ is direction-aware. Conversely, if $\beta \geq 1/2$, we can construct an adjacency matrix $\tilde{\mathbf{A}}$ such that $\lambda_{\min}(\mathbf{P}') \leq 0$ for some L . Let us assume that $L = 1$ and

$$\tilde{\mathbf{A}} := \begin{bmatrix} 0 & 1 \\ 1 & 0 \end{bmatrix}. \quad (25)$$

In this case, we have

$$\mathbf{P}' = (1-\beta)\mathbf{I} + \beta\tilde{\mathbf{A}} = \begin{bmatrix} 1-\beta & \beta \\ \beta & 1-\beta \end{bmatrix}, \quad (26)$$

whose eigenvalues are 1 and $1-2\beta$. The latter is non-positive for any $\beta \geq 1/2$.

□

REMARK 2. *The construction of $\tilde{\mathbf{A}}$ in Eq. (25) is not unique. In fact, any bipartite graph can be used as a counterexample.*

COROLLARY A.5 (THE PROOF OF THEOREM 2.1). *The iterative approximation is direction-aware for all possible normalized adjacency matrices and $L \geq 0$, if and only if $\beta < 1/2$. In contrast, the Neumann series approximation*

$$\hat{\psi}_{nsa}(\Delta\mathbf{E}) = (1-\beta) \sum_{l=0}^L \beta^l \tilde{\mathbf{A}}^l \Delta\mathbf{E}, \quad (27)$$

is structure-aware and direction-aware for any $\beta \in [0, 1)$.

PROOF. This is a corollary of Proposition A.2 and Proposition A.4. □

PROPOSITION A.6. *The rescaled Neumann series approximation $\hat{\psi}$ is structure-aware and direction-aware, and converges to the optimal solution as L increases.*

PROOF. The convergence to the optimal solution is obvious by noting that

$$\begin{aligned} \lim_{L \rightarrow +\infty} \hat{\psi}(\Delta \mathbf{E}) &= \lim_{L \rightarrow +\infty} \frac{1}{1-\beta^{L+1}} \cdot \lim_{L \rightarrow +\infty} \hat{\psi}_{nsa}(\Delta \mathbf{E}) \\ &= 1 \cdot \psi^*(\Delta \mathbf{E}) = \psi^*(\Delta \mathbf{E}). \end{aligned} \quad (28)$$

Similar to Proposition A.2, it can be proved that $\frac{1}{1-\beta^{L+1}} \mathbf{P}$ is positive definite with a largest eigenvalue ≤ 1 . Therefore, the rescaled transformation is also structure-aware and direction-aware. \square

A.2 Convergence Analysis

Before delving into the proof of the convergence, we would like to claim that the lemmas below are well known and can be found in most textbooks [1, 31] on convex optimization. For the sake of completeness, we provide here these proofs. Hereinafter, we use $\|\mathbf{X}\|_2$ to denote the spectral norm which returns the largest singular value of the matrix \mathbf{X} .

LEMMA A.7. *For a 2-times continuously differentiable function $f: \mathbb{R}^n \rightarrow \mathbb{R}$ with $\|\nabla^2 f(\mathbf{x})\|_2 \leq C$, $\forall \mathbf{x} \in \text{dom}(f)$, we have*

$$f(\mathbf{y}) \leq f(\mathbf{x}) + \langle \nabla f(\mathbf{x}), \mathbf{y} - \mathbf{x} \rangle + \frac{C}{2} \|\mathbf{y} - \mathbf{x}\|_2^2. \quad (29)$$

PROOF. For a Taylor expansion of $f(\mathbf{x})$, there exists a $\mathbf{z} = \tau \mathbf{x} + (1-\tau)\mathbf{y}$ for some $\tau \in [0, 1]$ such that

$$\begin{aligned} f(\mathbf{y}) &= f(\mathbf{x}) + \langle \nabla f(\mathbf{x}), \mathbf{y} - \mathbf{x} \rangle + \frac{(\mathbf{y} - \mathbf{x})^T \nabla^2 f(\mathbf{z})(\mathbf{y} - \mathbf{x})}{2} \\ &\leq f(\mathbf{x}) + \langle \nabla f(\mathbf{x}), \mathbf{y} - \mathbf{x} \rangle + \frac{C}{2} \|\mathbf{y} - \mathbf{x}\|_2^2. \end{aligned} \quad \square$$

LEMMA A.8. *For a positive definite matrix \mathbf{P} , let $\|\mathbf{x}\|_{\mathbf{P}} := (\mathbf{x}^T \mathbf{P} \mathbf{x})^{1/2}$ be the quadratic norm induced from \mathbf{P} . If the eigenvalues of \mathbf{P} fall into $[a, b]$, then*

$$\|\mathbf{P}\mathbf{x}\|_2^2 \leq b \|\mathbf{x}\|_{\mathbf{P}}^2, \quad a \|\mathbf{x}\|_2^2 \leq \|\mathbf{x}\|_{\mathbf{P}}^2. \quad (30)$$

PROOF. Firstly,

$$\|\mathbf{P}\mathbf{x}\|_2 = \|\mathbf{P}^{1/2} \mathbf{P}^{1/2} \mathbf{x}\|_2 \leq \|\mathbf{P}^{1/2}\|_2 \|\mathbf{x}\|_{\mathbf{P}} \leq \sqrt{b} \|\mathbf{x}\|_{\mathbf{P}}.$$

Secondly,

$$\|\mathbf{x}\|_2 = \|\mathbf{P}^{-1/2} \mathbf{P}^{1/2} \mathbf{x}\|_2 \leq \|\mathbf{P}^{-1/2}\|_2 \|\mathbf{x}\|_{\mathbf{P}} \leq \frac{1}{\sqrt{a}} \|\mathbf{x}\|_{\mathbf{P}}. \quad \square$$

THEOREM A.9. *Let $f: \mathbb{R}^n \times \mathbb{R}^m \rightarrow \mathbb{R}$ be a 2-times continuously differentiable function bounded below, and its Hessian matrix satisfies*

$$\|\nabla^2 f(\mathbf{x}, \mathbf{y})\|_2 \leq C, \quad \forall (\mathbf{x}, \mathbf{y}) \in \text{dom}(f) \quad (31)$$

for some constant C . The following gradient descent scheme is used to train \mathbf{x}, \mathbf{y} :

$$\mathbf{x}_{t+1} \leftarrow \mathbf{x}_t - \eta \mathbf{P} \nabla_{\mathbf{x}} f(\mathbf{x}_t, \mathbf{y}_t), \quad (32)$$

$$\mathbf{y}_{t+1} \leftarrow \mathbf{y}_t - \eta' \nabla_{\mathbf{y}} f(\mathbf{x}_t, \mathbf{y}_t), \quad (33)$$

where \mathbf{P} is deduced from the L -layer Neumann series approximation. Then, after T updates, we have,

$$\min_{t \leq T} \|\nabla f(\mathbf{x}_t, \mathbf{y}_t)\|_2^2 \leq \frac{2C}{\gamma(T+1)} \epsilon, \quad (34)$$

where $\epsilon = f(\mathbf{x}, \mathbf{y}) - f(\mathbf{x}^*, \mathbf{y}^*)$ and

$$\gamma = \begin{cases} \frac{1-\beta}{1+\beta} (1-\beta^L)(1+\beta^{L+1}), & \text{if } \eta = \eta' = \frac{1}{C} \\ \frac{1-\beta}{1+\beta} \frac{1-\beta^L}{1-\beta^{L+1}}, & \text{otherwise} \end{cases}.$$

PROOF. The update formula (32) can be unified into

$$\mathbf{z}_{t+1} := \begin{bmatrix} \mathbf{x}_{t+1} \\ \mathbf{y}_{t+1} \end{bmatrix} = \begin{bmatrix} \mathbf{x}_t \\ \mathbf{y}_t \end{bmatrix} - \underbrace{\begin{bmatrix} \eta \mathbf{P} & 0 \\ 0 & \eta' \mathbf{I} \end{bmatrix}}_{=: \tilde{\mathbf{P}}} \nabla f(\mathbf{x}_t, \mathbf{y}_t).$$

It is easy to show that

$$\begin{aligned} a &:= \min\left(\frac{1-\beta}{1+\beta} (1-\beta^L)\eta, \eta'\right) \leq \lambda_{\min}(\tilde{\mathbf{P}}) \\ &\leq \lambda_{\max}(\tilde{\mathbf{P}}) = \max((1-\beta^{L+1})\eta, \eta') =: b. \end{aligned}$$

Specifically,

$$\begin{aligned} a &= \begin{cases} \frac{1-\beta}{1+\beta} (1-\beta^L) \frac{1}{C}, & \text{if } \eta = \eta' = \frac{1}{C} \\ \frac{1-\beta}{1+\beta} \frac{1-\beta^L}{1-\beta^{L+1}} \frac{1}{C}, & \text{otherwise} \end{cases}, \\ b &= \begin{cases} (1-\beta^{L+1}) \frac{1}{C}, & \text{if } \eta = \eta' = \frac{1}{C} \\ \frac{1}{C}, & \text{otherwise} \end{cases}. \end{aligned}$$

In view of Lemma A.7 and Lemma A.8, we have

$$\begin{aligned} f(\mathbf{z}_{t+1}) &\leq f(\mathbf{z}_t) - \langle \nabla f(\mathbf{z}_t), \tilde{\mathbf{P}} \nabla f(\mathbf{z}_t) \rangle + \frac{C}{2} \|\tilde{\mathbf{P}} \nabla f(\mathbf{z}_t)\|_2^2 \\ &= f(\mathbf{z}_t) - \|\nabla f(\mathbf{z}_t)\|_{\tilde{\mathbf{P}}}^2 + \frac{C}{2} \|\tilde{\mathbf{P}} \nabla f(\mathbf{z}_t)\|_2^2 \\ &\leq f(\mathbf{z}_t) - \|\nabla f(\mathbf{z}_t)\|_{\tilde{\mathbf{P}}}^2 + \frac{bC}{2} \|\nabla f(\mathbf{z}_t)\|_{\tilde{\mathbf{P}}}^2 \end{aligned} \quad (35)$$

$$\begin{aligned} &= f(\mathbf{z}_t) - \left(1 - \frac{bC}{2}\right) \|\nabla f(\mathbf{z}_t)\|_{\tilde{\mathbf{P}}}^2 \\ &\leq f(\mathbf{z}_t) - a \left(1 - \frac{bC}{2}\right) \|\nabla f(\mathbf{z}_t)\|_2^2. \end{aligned} \quad (36)$$

Denoted by

$$\begin{aligned} \gamma &:= aC(2-bC) \\ &= \begin{cases} \frac{1-\beta}{1+\beta} (1-\beta^L)(1+\beta^{L+1}), & \text{if } \eta = \eta' = \frac{1}{C} \\ \frac{1-\beta}{1+\beta} \frac{1-\beta^L}{1-\beta^{L+1}}, & \text{otherwise} \end{cases}, \end{aligned} \quad (37)$$

we have

$$\begin{aligned} &\min_{0 \leq t \leq T} \|\nabla f(\mathbf{x}_t, \mathbf{y}_t)\|_2^2 \\ &\leq \frac{1}{T+1} \sum_{t=0}^T \|\nabla f(\mathbf{x}_t, \mathbf{y}_t)\|_2^2 \\ &\leq \frac{1}{T+1} \sum_{t=0}^T \frac{2C}{\gamma} (f(\mathbf{x}_t, \mathbf{y}_t) - f(\mathbf{x}_{t+1}, \mathbf{y}_{t+1})) \\ &= \frac{2C}{\gamma(T+1)} (f(\mathbf{x}_0, \mathbf{y}_0) - f(\mathbf{x}_{T+1}, \mathbf{y}_{T+1})) \\ &\leq \frac{2C}{\gamma(T+1)} \epsilon. \end{aligned} \quad \square$$

THEOREM A.10 (THE PROOF OF THEOREM 2.2). *If $\eta = \eta' = 1/C$, after T updates, we have*

$$\min_{t \leq T} \|\nabla \mathcal{L}(\mathbf{E}_t, \boldsymbol{\theta}_t)\|_2^2 = \mathcal{O}(C/((1-\beta)^2 T)). \quad (38)$$

If we adopt a modified learning rate for embedding:

$$\eta = \frac{1}{(1-\beta^{L+1})C}, \quad (39)$$

the convergence rate could be improved to $\mathcal{O}(C/((1-\beta)T))$.

PROOF. This is true for $L = 0$, since in this case the update mechanism becomes a normal gradient descent regardless of $\eta = 1/C$ or $\eta = \frac{1}{(1-\beta)C}$. Let us prove a general case for $L \geq 1$ next.

According to Theorem A.9, we have

$$\min_{t \leq T} \|\nabla \mathcal{L}(\mathbf{E}_t, \boldsymbol{\theta}_t)\|_2^2 \leq \frac{2C}{\gamma(T+1)} \epsilon,$$

where $\epsilon = \mathcal{L}(\mathbf{E}, \boldsymbol{\theta}) - \mathcal{L}(\mathbf{E}^*, \boldsymbol{\theta}^*)$ and

$$\gamma = \begin{cases} \frac{1-\beta}{1+\beta} (1-\beta^L)(1+\beta^{L+1}), & \text{if } \eta = \eta' = \frac{1}{C} \\ \frac{1-\beta}{1+\beta} \frac{1-\beta^L}{1-\beta^{L+1}}, & \text{otherwise} \end{cases}.$$

Notice that, for $\eta = \eta' = 1/C$,

$$\begin{aligned} \lim_{\beta \rightarrow 1} \frac{1/\gamma}{1/(1-\beta)^2} &= \lim_{\beta \rightarrow 1} \frac{\frac{1}{\frac{1-\beta}{1+\beta} (1-\beta^L)(1+\beta^{L+1})}}{\frac{1}{(1-\beta)^2}} \\ &= \lim_{\beta \rightarrow 1} \frac{1-\beta}{1-\beta^L} = \frac{1}{L}, \end{aligned} \quad (40)$$

and for $\eta = \frac{1}{(1-\beta^{L+1})C}$, $\eta' = \frac{1}{C}$,

$$\begin{aligned} \lim_{\beta \rightarrow 1} \frac{1/\gamma}{1/(1-\beta)} &= \lim_{\beta \rightarrow 1} \frac{\frac{1}{\frac{1-\beta}{1+\beta} \frac{1-\beta^L}{1-\beta^{L+1}}}}{\frac{1}{1-\beta}} \\ &= 2 \cdot \lim_{\beta \rightarrow 1} \frac{1-\beta^{L+1}}{1-\beta^L} = \frac{2(L+1)}{L}. \end{aligned} \quad (41)$$

Therefore,

$$\frac{1}{\gamma} = \begin{cases} \mathcal{O}(1/(1-\beta)^2), & \text{if } \eta = \eta' = \frac{1}{C} \\ \mathcal{O}(1/(1-\beta)), & \text{if } \eta = \frac{1}{(1-\beta^{L+1})C}, \eta' = \frac{1}{C} \end{cases}.$$

The rest of the proof is obvious. \square

A.3 Proofs of SEvo-enhanced AdamW

Adam(W) [22] uses the bias-corrected moment estimates for updating because they are unbiased when the actual moments are stationary throughout the training. Below, Lemma A.11 formally elaborates on this, and Theorem A.13 extends Theorem 3.2 with a proof of unbiasedness.

LEMMA A.11 ([22]). *Denoted by $\hat{\mathbf{m}}_t = \mathbf{m}_t/(1-\beta_1^t)$ and $\hat{\mathbf{v}}_t = \mathbf{v}_t/(1-\beta_2^t)$ the bias-corrected estimates, if the first and second moments are stationary, i.e.,*

$$\mathbb{E}[\mathbf{g}_t] = \mathbb{E}[\mathbf{g}], \quad \mathbb{E}[\mathbf{g}_t^2] = \mathbb{E}[\mathbf{g}^2], \quad \forall t = 1, 2, \dots,$$

then these bias-corrected estimates are unbiased:

$$\mathbb{E}[\hat{\mathbf{m}}_t] = \mathbb{E}[\mathbf{g}], \quad \mathbb{E}[\hat{\mathbf{v}}_t] = \mathbb{E}[\mathbf{g}^2], \quad \forall t = 1, 2, \dots$$

PROPOSITION A.12. *If a node is no longer sampled in subsequent p batches after step t , we have*

$$\Delta \mathbf{e}_{t+p-1} = \kappa \cdot \frac{\beta_1^p}{\sqrt{\beta_2^p}} \Delta \mathbf{e}_{t-1}, \quad (42)$$

where the coefficient of κ is mainly determined by t .

PROOF. In this case, the iterative formula becomes

$$\mathbf{m}_{t+j} = \beta_1^j \mathbf{m}_t + \mathbf{0},$$

$$\mathbf{v}_{t+j} = \beta_2^j \mathbf{v}_t + \mathbf{0},$$

$$\forall j = 0, 1, \dots, p.$$

Therefore,

$$\begin{aligned} \Delta \mathbf{e}_{t+p-1} &= \frac{\hat{\mathbf{m}}_{t+p}}{\sqrt{\hat{\mathbf{v}}_{t+p}}} = \frac{\sqrt{1-\beta_2^{t+p}}}{1-\beta_1^{t+p}} \frac{\mathbf{m}_{t+p}}{\sqrt{\mathbf{v}_{t+p}}} \\ &= \frac{\sqrt{1-\beta_2^{t+p}}}{1-\beta_1^{t+p}} \frac{\beta_1^p}{\sqrt{\beta_2^p}} \frac{\mathbf{m}_t}{\sqrt{\mathbf{v}_t}} = \frac{\beta_1^p \sqrt{1-\beta_2^{t+p}}}{\sqrt{\beta_2^p} (1-\beta_1^{t+p})} \frac{\mathbf{m}_t}{\sqrt{\mathbf{v}_t}} \\ &= \frac{\beta_1^p (1-\beta_1^t) \sqrt{1-\beta_2^{t+p}}}{\sqrt{\beta_2^p} (1-\beta_1^{t+p}) \sqrt{1-\beta_2^t}} \frac{\hat{\mathbf{m}}_t}{\sqrt{\hat{\mathbf{v}}_t}} \\ &= \frac{\beta_1^p}{\sqrt{\beta_2^p}} \cdot \underbrace{\frac{(1-\beta_1^t) \sqrt{1-\beta_2^{t+p}}}{(1-\beta_1^{t+p}) \sqrt{1-\beta_2^t}}}_{=: \kappa} \Delta \mathbf{e}_{t-1}. \end{aligned}$$

It is easy to show that

$$\lim_{t \rightarrow +\infty} \kappa(t, p) = 1, \quad \forall \beta_1, \beta_2 \in [0, 1). \quad (43)$$

\square

THEOREM A.13 (THE PROOF OF THEOREM 3.2). *Under the same assumptions as in Lemma A.11 and Proposition 3.1, the bias-corrected estimates are unbiased and $\Delta \mathbf{e}_{t+p-1} = \Delta \mathbf{e}_{t-1}$ if the estimates are updated in the following manner when $\mathbf{g}_t = \mathbf{0}$,*

$$\mathbf{m}_t = \beta_1 \mathbf{m}_{t-1} + (1-\beta_1) \frac{1}{1-\beta_1^{t-1}} \mathbf{m}_{t-1}, \quad (44)$$

$$\mathbf{v}_t = \beta_2 \mathbf{v}_{t-1} + (1-\beta_2) \frac{1}{1-\beta_2^{t-1}} \mathbf{v}_{t-1}. \quad (45)$$

PROOF. We first show the unbiasedness of \mathbf{m}_t and the proof for \mathbf{v}_t is completely analogous. It remains only to show that

$$\mathbb{E}[\mathbf{m}_t] = (1-\beta_1^t) \mathbb{E}[\mathbf{g}].$$

This is trivial for $t = 0$. Assuming that this also holds in the case of $t-1$, it can be proved by induction.

If $\mathbf{g}_t \neq \mathbf{0}$,

$$\begin{aligned} \mathbb{E}[\mathbf{m}_t] &= \beta_1 \mathbb{E}[\mathbf{m}_{t-1}] + (1-\beta_1) \mathbb{E}[\mathbf{g}_t] \\ &= \beta_1 (1-\beta_1^{t-1}) \mathbb{E}[\mathbf{g}] + (1-\beta_1) \mathbb{E}[\mathbf{g}] \\ &= (1-\beta_1^t) \mathbb{E}[\mathbf{g}]. \end{aligned}$$

If $\mathbf{g}_t = \mathbf{0}$,

$$\begin{aligned}\mathbb{E}[\mathbf{m}_t] &= \beta_1 \mathbb{E}[\mathbf{m}_{t-1}] + (1 - \beta_1) \frac{1}{1 - \beta_1^{t-1}} \mathbb{E}[\mathbf{m}_{t-1}] \\ &= \frac{1 - \beta_1^t}{1 - \beta_1^{t-1}} \mathbb{E}[\mathbf{m}_{t-1}] = (1 - \beta_1^t) \mathbb{E}[\mathbf{g}].\end{aligned}$$

If the node is no longer sampled in subsequent p batches after step t , we have

$$\begin{aligned}\mathbf{m}_{t+j} &= \beta_1 \mathbf{m}_{t+j-1} + (1 - \beta_1) \frac{1}{1 - \beta_1^{t+j-1}} \mathbf{m}_{t+j-1} \\ &= \frac{1 - \beta_1^{t+j}}{1 - \beta_1^{t+j-1}} \mathbf{m}_{t+j-1} \\ &= \frac{1 - \beta_1^{t+j}}{1 - \beta_1^{t+j-1}} \frac{1 - \beta_1^{t+j-1}}{1 - \beta_1^{t+j-2}} \mathbf{m}_{t+j-2} \\ &= \dots = \frac{1 - \beta_1^{t+j}}{1 - \beta_1^t} \mathbf{m}_t, \quad \forall j = 1, 2, \dots, p.\end{aligned}$$

Analogously, we have,

$$\mathbf{v}_{t+j} = \frac{1 - \beta_2^{t+j}}{1 - \beta_2^t} \mathbf{v}_t, \quad \forall j = 1, 2, \dots, p.$$

Therefore, the conclusion can be deduced from

$$\begin{aligned}\hat{\mathbf{m}}_{t+p} &= \frac{1}{1 - \beta_1^{t+p}} \mathbf{m}_{t+p} = \frac{1}{1 - \beta_1^t} \mathbf{m}_t = \hat{\mathbf{m}}_t, \\ \hat{\mathbf{v}}_{t+p} &= \frac{1}{1 - \beta_2^{t+p}} \mathbf{v}_{t+p} = \frac{1}{1 - \beta_2^t} \mathbf{v}_t = \hat{\mathbf{v}}_t.\end{aligned}$$

□

B ALGORITHMS

We present the algorithms of SEvo-enhanced SGD and Adam in Algorithm 2 and Algorithm 3, respectively.

Algorithm 2: SGD with momentum enhanced by SEvo. Differences from the original SGD are colored in blue. The matrix operation below are element-wise.

Input: embedding matrix \mathbf{E} , learning rate η , momentum factors $\mu, \beta \in [0, 1)$, weight decay λ .

foreach step t **do**

$\mathbf{G}_t \leftarrow \nabla_{\mathbf{E}} \mathcal{L} + \lambda \mathbf{E}_{t-1};$ // Get gradients

$\mathbf{M}_t \leftarrow \mu \mathbf{M}_{t-1} + \mathbf{G}_t;$ // Moment update

Update via SEvo:

$$\mathbf{E}_t \leftarrow \mathbf{E}_{t-1} - \eta \hat{\psi}(\mathbf{M}_t; \beta).$$

Output: optimized embeddings \mathbf{E} .

Algorithm 3: Adam enhanced by SEvo. Differences from the original Adam are colored in blue. The matrix operation below are element-wise.

Input: embedding matrix \mathbf{E} , learning rate η , momentum factors $\beta_1, \beta_2, \beta \in [0, 1)$, weight decay λ .

foreach step t **do**

$\mathbf{G}_t \leftarrow \nabla_{\mathbf{E}} \mathcal{L} + \lambda \mathbf{E}_{t-1};$ // Get gradients

Update first/second moment estimates:

$$\mathbf{M}_t \leftarrow \beta_1 \mathbf{M}_{t-1} + (1 - \beta_1) \mathbf{G}_t,$$

$$\mathbf{V}_t \leftarrow \beta_2 \mathbf{V}_{t-1} + (1 - \beta_2) \mathbf{G}_t^2;$$

Compute bias-corrected first/second moment estimates:

$$\hat{\mathbf{M}}_t \leftarrow \mathbf{M}_t / (1 - \beta_1^t),$$

$$\hat{\mathbf{V}}_t \leftarrow \mathbf{V}_t / (1 - \beta_2^t);$$

Update via SEvo:

$$\mathbf{E}_t \leftarrow \mathbf{E}_{t-1} - \eta \hat{\psi}(\hat{\mathbf{M}}_t / \sqrt{\hat{\mathbf{V}}_t + \epsilon}; \beta).$$

Output: optimized embeddings \mathbf{E} .

C BASELINES

Four GNN-based baselines for performance and efficiency benchmarks:

- **LightGCN** [15] is a pioneering collaborative filtering model that simplifies graph convolutional networks (GCNs) by removing nonlinearities for easier training. It uses only graph structure information and has no access to sequence information.
- **SR-GNN** [45] and **LESSR** [7] are two baselines dynamically constructing session graph. The former employs a gated graph neural network to obtain the final node vectors, while the latter utilizes edge-order preserving multigraph and a shortcut graph to address the lossy session encoding and ineffective long-range dependency capturing problems, respectively.
- **MAERec** [48] learns to sample less noisy paths from a semantic similarity graph for subsequent reconstruction tasks. However, we found that the official implementation treats the recommendation loss and reconstruction loss equally, leading to poor performance here. Therefore, an additional weight is attached to the reconstruction loss and a grid search is performed in the range of $[0, 1]$. Almost all hyperparameters are tuned for competitive performance.

Four sequence backbones to validate the effectiveness of SEvo:

- **GRU4Rec** [16] applies RNN [8] to recommendation with specific modifications made to cope with data sparsity. In addition to the learning rate in $\{1e-4, 5e-4, 1e-3, 5e-3\}$ and weight decay in $[0, 0.1]$, we also tune the dropout rate for node features in the range of $[0, 0.7]$.
- **SASRec** [21] and **BERT4Rec** [38] are two pioneering works on sequential recommendation equipped with unidirectional and bidirectional self-attention, respectively. For BERT4Rec which employs a separate fully-connected layer for scoring, the weight matrix therein will also be smoothed by SEvo. In addition to

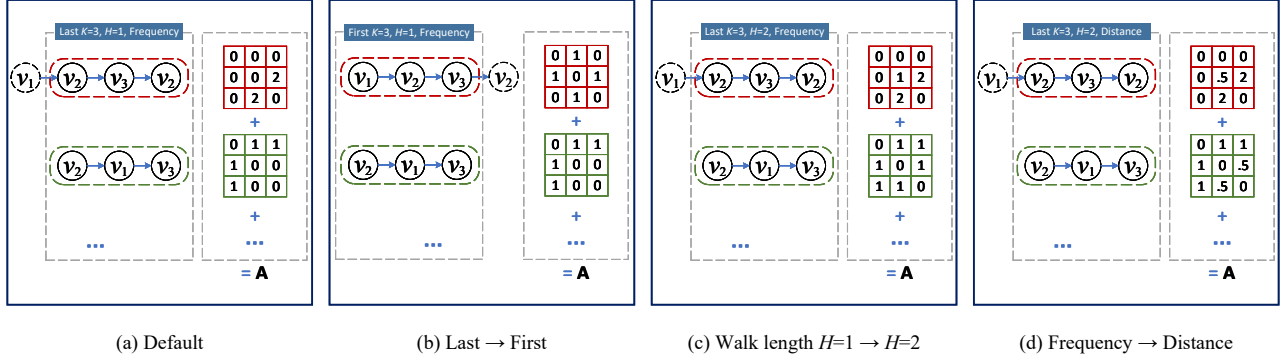


Figure 5: Illustrations of different pairwise similarity estimation methods based on interaction data. (a) The default is to adopt the co-occurrence frequency within the last K items. (b) Using only the first K items. (c) Allowing a maximum walk length of H beyond 1. (d) Frequency-based similarity versus distance-based similarity.

some basic hyperparameters, the mask ratio is also researched for BERT4Rec.

- **STOSA** [12] is one of the state-of-the-art models. It aims to capture the uncertainty of sequential behaviors by modeling each item as a Gaussian distribution. The hyperparameters involved are tuned similarly to SASRec.

Four knowledge distillation methods used in Appendix D.3:

- **KD** [17] and **DKD** [51] are two logits-based approaches to transfer knowledge. DKD decomposes the classical KD loss into target class knowledge distillation loss and non-target class knowledge distillation loss.
- **RKD** [32] and **HTD** [20] are two ranking-based approaches. The former focuses the distillation of relational knowledge through distance-wise and angle-wise alignments, while the latter emphasizes the distillation of hierarchical topology by dividing nodes into multiple groups and requiring intra-group and inter-group alignments.

D PAIRWISE SIMILARITY ESTIMATION

Here, we preliminarily explore the exploitation of more types of knowledge besides consecutive occurrences. We first investigate some elementary factors for interaction data, and then introduce the applications of SEvo to node categories and knowledge distillation.

D.1 SEvo for Interaction Data

Recent GNN-based sequence models [45, 46], as well as the SEvo-enhanced models in Section 4, estimate the pairwise similarity w_{ij} between items v_i and v_j based on their co-occurrence frequency in sequences. In other words, items that appear consecutively more often are assumed more related. Yet there are some factors that deserve a closer look:

- The maximum sequence length K for construction to investigate the number of interactions required for accurate estimation.
- Using only the first K versus last K interactions in each sequence to compare the utility of early and recent preferences.

Algorithm 4: Python-style algorithm for similarity estimation based on interaction data.

```

for seq in seqs:
    if first:
        seq = seq[:K] # First K items
    else:
        seq = seq[-K:] # Last K items
    for i in range(len(seq) - 1):
        # Maximum walk length H
        for h, j in enumerate(
            range(i + 1, min(i + H + 1,
                len(seq))),
            start=1
        ):
            if frequency: # Frequency
                A[seq[i], seq[j]] += 1
                A[seq[j], seq[i]] += 1
            else: # Distance
                A[seq[i], seq[j]] += 1 / h
                A[seq[j], seq[i]] += 1 / h

```

- Allowing related items to be connected by a walk of length $\leq H$ rather than strict consecutive occurrences.

- Frequency-based similarity versus distance-based similarity. The former weights all related pairs equally, while the latter weights inversely to their walk length. For example, given a sequence $v_2 \rightarrow v_1 \rightarrow v_3$ with a maximum walk length of $H = 2$, the frequency-based similarity of (v_2, v_3) gives 1, while the distance-based similarity is $1/2$ (as the walk length from v_2 to v_3 is 2).

Figure 5 illustrates these four variants and Algorithm 4 details a step-by-step process.

We empirically compare these four potential factors in Figure 6:

- Figure 6a shows the effect of confining the maximum sequence length to the **first/last** K items, so only the **early/recent** preferences will be considered. In contrast to early interactions, recent

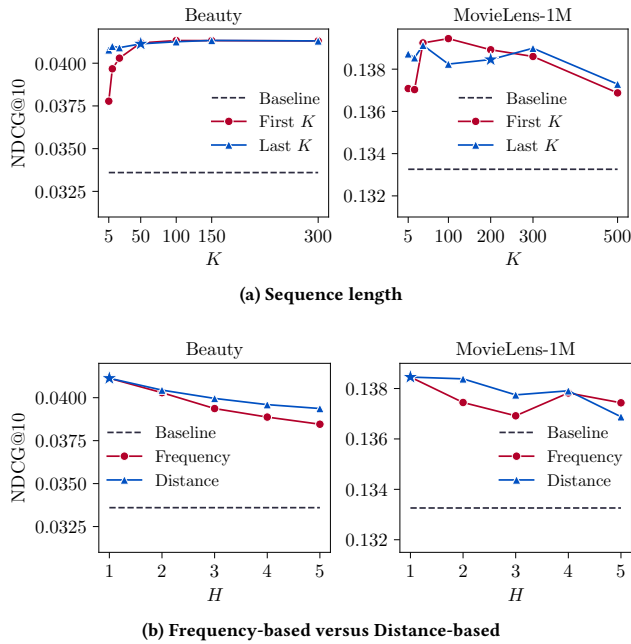


Figure 6: Comparison of similarity estimation across four potential factors. ‘★’ indicates the default way applied to SEvo-enhanced sequence models in Section 4.2. (a) Using only the first/last K items for pairwise similarity estimation. (b) Frequency- and distance-based similarity with a maximum walk length of H .

ones imply more precise pairwise relations for future prediction, even for small K . With the increasing of the maximum sequence length, the recommendation performance on Beauty increases steadily, but not the case for MovieLens-1M. This suggests that shopping relations may be more consistent than movie preferences. The latter may be more diverse among different users. Excessively long sequences cause the similarity estimation to be skewed toward the tastes of mass viewing users.

- Figure 6b explores the relations beyond strict consecutive occurrences; that is, two items are considered related once they co-occur within a path of length $\leq H$. For the shopping and movie datasets, estimating similarity beyond co-occurrence frequency appears less reliable overall. We also compare frequency-based similarity with distance-based similarity that decreases weights for more distant pairs. It is clear that the distance-based approach performs more stable as the maximum walk length H increases.

D.2 SEvo for Node Categories

Sometimes embeddings are expected to be smooth w.r.t. a prior knowledge. For example, in addition to the interaction data, each movie in the MovieLens-1M dataset is associated with at least one genre. It is natural to assume that movies of the same genre are related to each other. Heuristically, we can define the similarity w_{ij} to be 1 if v_i and v_j belong to the same genre and 0 otherwise.

Table 6: Pairwise similarity estimation based on interaction data versus node categories (movie genres).

	β	MovieLens-1M		
		HR@1	HR@10	NDCG@10
Baseline (SASRec)	0	0.0457	0.2482	0.1315
Interaction data	0.5	0.0494	0.2538	0.1362
	0.99	0.0517	0.2567	0.1385
Movie genres	0.5	0.0492	0.2527	0.1352
	0.99	0.0508	0.2549	0.1371

As can be seen in Figure 7, such smoothness constraint can also be fulfilled through SEvo, leading to progressively stronger clustering effects as β increases. However, the resulting performance gains are slightly less than those based on interaction data (see Table 6). One possible reason is that the viewing order is interest rather than genre oriented, and the movie genres are too coarse to provide particularly useful information. In conclusion, while smoothness is an appealing inductive bias, its utility depends on how well the imposed structure information agrees with the performance metrics of interest.

D.3 SEvo for Knowledge Distillation

Table 7: Knowledge distillation from Teacher (SASRec with a embedding size of 200) to Student (SASRec with a embedding size of 20). The results are averaged over 5 independent runs on the Beauty dataset.

	HR@1	HR@5	HR@10	NDCG@5	NDCG@10
Teacher	0.0198	0.0544	0.0786	0.0374	0.0452
Student	0.0094	0.0327	0.0526	0.0210	0.0275
+KD [17]	0.0105	0.0352	0.0552	0.0229	0.0294
+RKD [32]	0.0082	0.0311	0.0515	0.0196	0.0262
+HTD [20]	0.0085	0.0344	0.0549	0.0215	0.0281
+DKD [51]	0.0138	0.0389	0.0577	0.0265	0.0325
Student	0.0094	0.0327	0.0526	0.0210	0.0275
+SEvo	0.0107	0.0364	0.0576	0.0236	0.0304
+DKD	0.0166	0.0407	0.0568	0.0289	0.0341

In addition to the affinity matrix extracted from interaction data or relation data, the pairwise similarity can also be estimated from a heavy-weight teacher model. Recall that Knowledge Distillation (KD) [17] encourages a light-weight student model to mimic the behaviors (e.g., output distribution) of the teacher model, so the learned student model achieves both accuracy and efficiency. In general, higher-dimensional embeddings are capable of better fitting the underlying distribution between entities. The pairwise similarities extracted from a teacher model, needless to say, can be used to guide the embedding evolution of a student model. Unlike interaction or relation data, the deduced graph is dense if only the distance function is applied. Therefore, some graph construction steps including sparsification and reweighting should be involved as well. We attempt to use the widely used KNN graph here, and

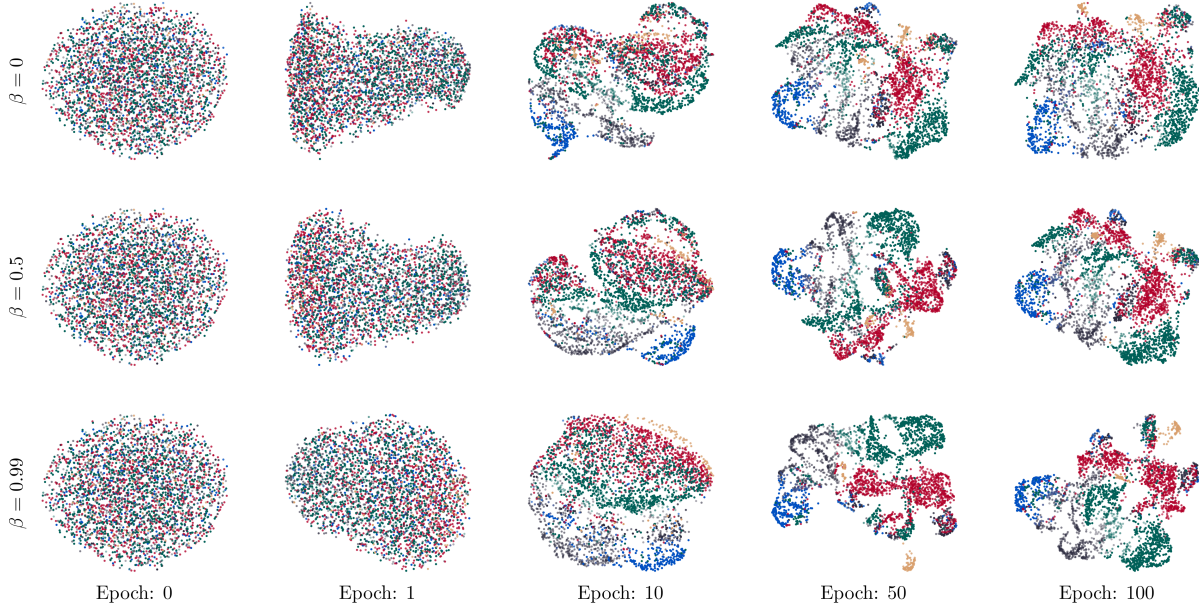


Figure 7: UMAP [29] visualization of movies based on their embeddings. For ease of differentiation, we group the 18 genres into 6 categories and colored them individually: Thriller/Crime/Action/Adventure; Horror/Mystery/Film-Noir; War/Drama/Romance; Comedy/Musical/Children’s/Animation; Fantasy/Sci-Fi; Western/Documentary.

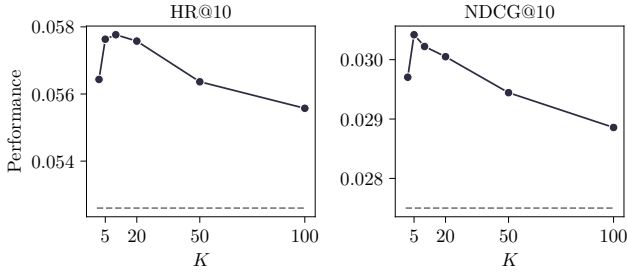


Figure 8: Knowledge distillation by SEvo across different top- K neighbors. The dashed line indicates the result of the student model.

leave a more comprehensive study of graph construction [19] as a future work.

Specifically, the distance between each pair v_i, v_j is estimated using a cosine similarity distance function:

$$d_{ij} = \frac{\mathbf{e}_i^T \mathbf{e}_j}{\|\mathbf{e}_i\|_2 \|\mathbf{e}_j\|_2}. \quad (46)$$

Then, K -nearest neighbors are selected for each node; that is

$$(i, j) \in \mathcal{E}, i \neq j \text{ iff } |\{k \neq i : d_{ik} \leq d_{ij}\}| \leq K. \quad (47)$$

This sparsification is necessary for several reasons: 1) SEvo with a dense adjacency matrix is computationally prohibitive to conduct; 2) Generally, only the top-ranked neighbors are reliable for next distillation. Finally, the adjacency matrix is obtained through

reweighting and symmetrizing:

$$w_{ij} = \hat{w}_{ij} + \hat{w}_{ji}, \quad \hat{w}_{ij} := \exp(-d_{ij}/\tau),$$

where $\tau > 0$ is the kernel bandwidth parameter.

Table 7 reports the results of the SASRec backbone with different embedding sizes (200 versus 20). Although a student equipped with SEvo can only derive guidance from the teacher in terms of embedding modeling, it has surpassed RKD and HTD that focus on feature/output alignments. Recall that SEvo only needs to access the teacher model once for adjacency matrix construction, whereas other knowledge distillation approaches require accessing the teacher model for each update. SEvo is arguably an efficient tool for transferring embedding knowledge. Nevertheless, SEvo alone cannot be expected to facilitate the learning of the other modules, which consequently is still inferior to state-of-the-art methods such as DKD. Fortunately, SEvo and DKD can work together to further boost the recommendation performance.

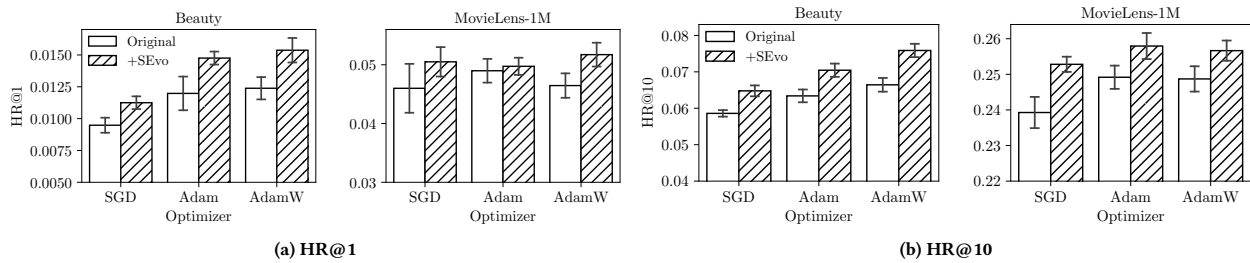
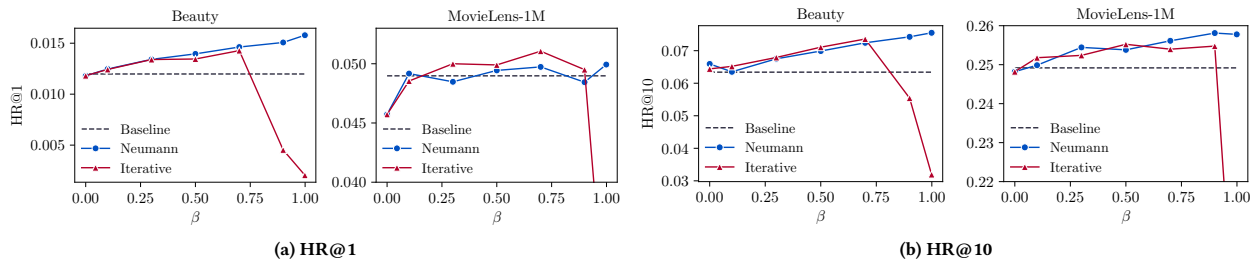
We also investigate the impact of top- K neighbors in Figure 8. Because the similarity estimation becomes less reliable as K increases, the benefits obtained from SEvo gradually diminish once $K > 10$. This observation is consistent with the idea [20] that blindly forcing the student model to mimic the teacher’s behavior is counterproductive.

E ADDITIONAL EXPERIMENTAL RESULTS

Additional experimental results are presented in this part, including the training and inference times on four datasets (Table 8), Hit Rate performance of various SEvo-enhanced optimizers (Figure 9), and Hit Rate comparison between different approximations (Figure 10).

Table 8: Training and inference times. The wall time (seconds) is evaluated on an Intel Xeon E5- 2620 v4 platform and a single GTX 1080Ti GPU.

		Beauty			Toys			Tools			MovieLens-1M		
		Training	Inference	Epochs	Training	Inference	Epochs	Training	Inference	Epochs	Training	Inference	Epochs
GNN	LightGCN	2000.50	1.07	1000	1461.14	0.97	900	922.60	0.78	600	6898.42	1.95	600
	SR-GNN	25837.60	14.52	300	13711.61	11.82	200	9455.18	12.23	150	126129.93	6.16	150
	LESSR	19686.60	14.35	300	15923.59	9.67	300	10994.38	8.30	300	203226.08	5.02	300
	MAERec	23956.43	3.60	100	43233.90	2.60	200	16920.16	2.31	100	42586.58	2.41	200
MF or RNN/Transformer	MF-BPR	1781.65	0.96	1000	1508.73	0.91	1000	1326.93	0.71	1000	6837.01	1.95	600
	+SEvo	1937.32	0.96	1000	1572.91	0.91	1000	1510.23	0.71	1000	7128.00	1.95	600
	GRU4Rec	927.98	1.98	300	646.51	1.77	300	638.57	1.65	300	12116.04	1.78	300
	+SEvo	987.47	1.98	300	791.19	1.77	300	661.83	1.65	300	12387.25	1.78	300
MF or RNN/Transformer	SASRec	445.68	2.16	200	413.35	2.30	200	353.10	1.81	200	919.27	1.24	200
	+SEvo	469.27	2.16	200	480.37	2.30	200	378.25	1.81	200	954.77	1.24	200
	BERT4Rec	1470.76	2.03	500	1330.58	1.71	500	1092.10	1.51	500	1131.62	1.18	500
	+SEvo	1965.97	2.03	500	1595.66	1.71	500	1374.72	1.51	500	1243.08	1.18	500
MF or RNN/Transformer	STOSA	2253.98	9.84	500	2049.00	8.42	500	1827.60	6.65	500	2220.18	1.98	500
	+SEvo	2491.54	9.84	500	2231.11	8.42	500	1879.62	6.65	500	2259.66	1.98	500

**Figure 9: Hit Rate performance of various SEvo-enhanced optimizers.****Figure 10: Hit Rate comparison between different approximations.**